

## SULFIDE EVOLUTION DURING PROGRADE METAMORPHISM OF THE OTAGO AND ALPINE SCHISTS, NEW ZEALAND

IAIN K. PITCAIRN<sup>§</sup>

*Department of Geology and Geochemistry, Stockholm University, SE-10691 Stockholm, Sweden*

GEMA R. OLIVO

*Department of Geological Sciences and Geological Engineering, Queen's University, Kingston, Ontario K7L 3N6, Canada*

DAMON A.H. TEAGLE

*School of Ocean and Earth Science, National Oceanography Centre, University of Southampton,  
 European Way, Southampton SO14 3ZH, U.K.*

DAVE CRAW

*Geology Department, University of Otago, PO Box 56, Dunedin, New Zealand*

### ABSTRACT

Sulfide minerals in the Otago and Alpine schists, New Zealand, a metasedimentary belt exposed from unmetamorphosed greywackes up to amphibolite facies, underwent systematic changes in abundance, composition and texture during prograde metamorphism. In unmetamorphosed rocks, the most common sulfide mineral is frambooidal pyrite, which contains abundant As (up to 14000 ppm), Co (up to 4000 ppm), Cu (up to 14000 ppm), Ni (up to 1100 ppm) and, locally, Ag (up to 270 ppm), Au (up to 90 ppm), and Sb (up to 240 ppm). Chalcopyrite, sphalerite, and galena also occur as isolated grains. Chalcopyrite and sphalerite contain few trace elements, whereas galena contains significant Se (up to 1600 ppm) and locally abundant Hg (up to 600 ppm). The distribution of these trace and minor elements is extremely heterogeneous. In subgreenschist-facies rocks, pyrrhotite replaces pyrite, and there is a clear textural change from frambooidal pyrite to composite grains of pyrrhotite, sphalerite, chalcopyrite, galena and cobaltite. Pyrrhotite contains Co (average values  $1100 \pm 490$  ppm), Cu (up to 17000 ppm), and Ni (up to 11000 ppm). Antimony and Hg are above detection in rare individual grains, but none of the other trace and minor elements sought are detectable. Sphalerite, galena and cobaltite increase in proportion in subgreenschist-facies rocks, and also contain higher concentrations of Ag (up to 1480 ppm in galena), Au (up to 230 ppm in galena and 110 ppm in cobaltite), As ( $38 \pm 6$  wt. % in cobaltite), Co ( $26 \pm 4$  wt. % in cobaltite), Hg (up to 4500 ppm in galena and 1100 ppm in sphalerite), and Sb (up to 1280 ppm in cobaltite and 770 ppm in galena). Pyrite, sphalerite, galena, and cobaltite become less abundant from subgreenschist- to amphibolite-facies rocks. In amphibolite-facies rocks, only pyrrhotite, chalcopyrite and trace amounts of galena and molybdenite occur, and none of these minerals contain detectable levels of Ag, Au, As, or Hg. Mass-balance calculations between sulfide minerals and whole rocks show that sulfides are important host minerals for S, Cu, and As, but host a minor proportion of Fe, Zn, and Pb. As pyrite, sphalerite, galena, and cobaltite become less abundant at higher metamorphic grade, Pb, Zn and Co are retained in the rock incorporated in other minerals, whereas As, Sb, Hg, Au, and Ag are removed from the rock, most likely by metamorphic devolatilization.

**Keywords:** sulfide minerals, metamorphism, orogenic gold, Otago Schists, Alpine Schists, New Zealand.

### SOMMAIRE

Les minéraux sulfurés des schistes des séries Otago et Alpine, en Nouvelle-Zélande, roches appartenant à une ceinture métasédimentaire contenant des grauwakes non métamorphisés jusqu'au équivalents au faciès amphibolite, ont subi des changements systématiques en abondance, composition et texture au cours du métamorphisme prograde. Dans les roches non métamorphisées, le sulfure le plus répandu est la pyrite framboïdale, qui contient beaucoup d'As (jusqu'à 14000 ppm), Co

<sup>§</sup> E-mail address: iain.pitcairn@geo.su.se

(jusqu'à 4000 ppm), Cu (jusqu'à 14000 ppm), Ni (jusqu'à 1100 ppm) et, localement, Ag (jusqu'à 270 ppm), Au (jusqu'à 90 ppm), et Sb (jusqu'à 240 ppm). Chalcopyrite, sphalérite, et galène sont aussi présentes en grains isolés. La chalcopyrite et la sphalérite ne contiennent que quelques éléments en traces, tandis que la galène peut contenir des quantités importantes de Se (jusqu'à 1600 ppm) et, localement, de Hg (jusqu'à 600 ppm). La distribution de ces éléments traces et mineurs s'avère extrêmement hétérogène. Déjà dans les roches de grade inférieur au faciès schistes verts, la pyrrhotite remplace la pyrite, et il y a un changement textural marqué de la pyrite framboïdale aux grains composites de pyrrhotite, sphalérite, chalcopyrite, galène et cobaltite. La pyrrhotite contient Co (valeurs moyennes  $1100 \pm 490$  ppm), Cu (jusqu'à 17000 ppm) et Ni (jusqu'à 11000 ppm). L'antimoine et le mercure dépassent le seuil de la détection dans certains cas individuels, mais aucun des autres éléments ciblés ne semble présent. Sphalérite, galène et cobaltite augmentent en proportion dans les roches légèrement métamorphisées, et ces minéraux contiennent aussi des teneurs plus élevées en Ag (jusqu'à 1480 ppm dans la galène), Au (jusqu'à 230 ppm dans la galène et 110 ppm dans la cobaltite), As (38 ± 6% dans la cobaltite), Co (26 ± 4% dans la cobaltite), Hg (jusqu'à 4500 ppm dans la galène et 1100 ppm dans la sphalérite), et Sb (jusqu'à 1280 ppm dans la cobaltite et 770 ppm dans la galène). Pyrite, sphalérite, galène, et cobaltite deviennent moins abondants avec augmentation du degré de métamorphisme. Dans les roches ayant atteint le faciès amphibolite, seuls pyrrhotite, chalcopyrite et des traces de galène et de molybdénite sont présentes, mais aucun de ces minéraux ne contient des quantités détectables de Ag, Au, As, ou Hg. Des calculs du bilan des masses entre minéraux sulfurés et roches globales montrent que les sulfures sont des hôtes importants de S, Cu, et As, et accommodent une proportion mineure de Fe, Zn, et Pb. A mesure que pyrite, sphalérite, galène et cobaltite deviennent moins abondants aux grades métamorphiques plus élevés, Pb, Zn et Co sont retenus dans la roche, incorporés dans d'autres minéraux, tandis que As, Sb, Hg, Au, et Ag sont éliminés des roches, tout probablement par dévolatilisation métamorphique.

(Traduit par la Rédaction)

**Mots-clés:** minéraux sulfurés, métamorphisme, orogénique, schistes d'Otago, schistes Alpine, Nouvelle-Zélande.

## INTRODUCTION

Sulfide minerals are widespread in sedimentary and metamorphic rocks, yet there have been few systematic studies of their textural and chemical evolution during metamorphism. Sulfide minerals are sensitive indicators of redox conditions during metamorphism, and they partially control the composition of metamorphic fluids (Rumble 1973, Spear 1993). These minerals are also a major host phase for a large number of minor and trace elements in sedimentary and metamorphic rocks, including S, Ag, Au, As, Co, Cu, Hg, Mo, Ni, Pb, Sb, Se, Sn, W, and Zn (Barton 1970, Raiswell & Plant 1980, Dill & Kemper 1990, Craig & Vokes 1993, Graham & Robertson 1995, Watson *et al.* 1995, Wilkin & Barnes 1997).

Very little is known about the evolution of minor and trace elements in sulfide minerals during metamorphism. An investigation of the compositional evolution of sulfide minerals is essential for a complete understanding of fluid–rock interaction in the crust, chemical cycling during metamorphism, and the sources of metals and metal-carrying ligands in ore-forming fluids. In this paper, we use transmitted and reflected light microscopy, scanning electron microscopy (SEM) and electron-microprobe analysis (EMPA) for *in situ* analysis of the minerals, combined with chemical data on whole-rock samples to investigate the textural and chemical variation of sulfide minerals in sedimentary and metamorphic rocks from the Otago and Alpine schists, New Zealand. These rocks, of Mesozoic age, comprise pelites and psammites with minor (<5%) metabasalts and metacherts. A full crustal section is exposed from unmetamorphosed greywackes to

amphibolite-facies schists (Mortimer 1993, 2000). Consequently, these rocks provide an ideal laboratory to investigate the textural and chemical changes of sulfide and oxide minerals during low- to middle-grade metamorphism.

## BACKGROUND INFORMATION

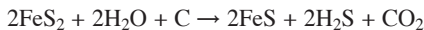
Previous investigators of sulfide minerals in metamorphic rocks have focused on oxide – silicate – sulfide – fluid equilibria in order to constrain  $f(O_2)$  and  $f(S_2)$  during metamorphism (Guidotti 1970, Thompson 1972, Itaya 1975, Ferry 1981, Hall 1986, Tracy & Robinson 1988, Poulson & Ohmoto 1989, Harlov *et al.* 1997, Harlov & Hansen 2005, Kawakami *et al.* 2006, Brown *et al.* 2006). A key aspect of these studies has been the evaluation of whether significant mass-transfer of sulfur occurs during metamorphism. Pyrite is commonly considered to be the most abundant sulfide mineral in marine sediments and sedimentary rocks (Sweeney & Kaplan 1963, Berner 1970, Raiswell & Plant 1980, Wilkin & Barnes 1997), whereas pyrrhotite is commonly the most abundant sulfide mineral in mid- to high-grade metasedimentary rocks (Carpenter 1974, Itaya 1975, Ferry 1981, Hall 1986, Kawakami *et al.* 2006). The pyrite-to-pyrrhotite desulfidation reaction has been mapped as broadly coinciding with the biotite isograd in pelitic schists from Tennessee and North Carolina, U.S.A. (Carpenter 1974), but has been suggested to occur at lower metamorphic temperatures in low- $f(O_2)$  conditions (Hall 1986). Thermodynamic modeling shows the stability of pyrite to be controlled partly by temperature and pressure, and partly by the amount of  $H_2O$  present, with the main release of sulfur

occurring over a narrow range of P–T conditions corresponding to breakdown of chlorite in the lower amphibolite facies (Tomkins 2010).

The degree of involvement of coexisting oxide and Fe–Mg silicate minerals in this reaction remains controversial. Compositions of coexisting Fe–Mg silicates are found to systematically vary with sulfide assemblage (Thompson 1972, Tracy & Robinson 1988, Harlov *et al.* 1997), implying local mobilization of sulfur during metamorphism by the following reaction:



However, where the volume of fluid created during prograde devolatilization is high, the reaction is likely to proceed *via* the removal of S through the reaction (Ferry 1981):



The sulfidation of pyrrhotite to pyrite is commonly observed in high-grade metamorphic rocks and is considered to be a retrograde reaction (Itaya 1975, Harlov *et al.* 1997, Harlov & Hansen 2005, Kawakami *et al.* 2006).

#### GEOLOGICAL SETTING OF THE OTAGO AND ALPINE SCHISTS

The Otago Schist forms part of a Mesozoic metasedimentary belt that arose through collision of the Torlesse and Caples terranes (Fig. 1; Coombs *et al.* 1976, Bishop *et al.* 1985, Mortimer 1993). The schists comprise quartzofeldspathic and volcanogenic metagreywackes and metapelites that have a broadly uniform composition over large volumes of rock, with minor metavolcanic and metachert horizons (Roser & Cooper 1990, Mortimer & Roser 1992). The mineralogical composition of the metasedimentary rocks is shown in Table 1. The metasedimentary rocks are interpreted to have formed as turbiditic sequences deposited in a tectonically active continental margin setting (MacKinnon 1983). The metamorphic grade ranges from unmetamorphosed Torlesse and Caples greywackes that crop out on the flanks of the schist belt to upper greenschist facies in the center of the belt (Fig. 1). The pressure and temperature of metamorphism are not well known, but maximum conditions for the Otago schists are estimated at 450°C and between 4.5 and 8 kbar (Jamieson & Craw 1987, Mortimer 1993, 2000). Dating using the Ar–Ar method suggests that the metamorphism of the Otago Schist occurred between 200 and 120 Ma (Little *et al.* 1999, Gray & Foster 2004). The timing of peak metamorphism is poorly known, but most likely occurred considerably later (~160–140 Ma) in higher-grade rocks than in lower-grade rocks (~180 Ma; Little *et al.* 1999, Gray & Foster 2004).

A change from strike-slip to transpressional tectonics along the Alpine Fault in the Miocene resulted in the uplift and exposure of the Alpine Schist (Fig. 1; Norris *et al.* 1990). These rocks are part of the Torlesse terrane (Roser & Cooper 1990), and range in metamorphic grade from chlorite-zone greenschist facies (450°C, 4.5–8 kbar) to garnet–oligoclase-zone amphibolite facies (Fig. 1; 600–650°C, 7–10 kbar; Grapes 1995, Mortimer 2000). The rapidity of the uplift resulted in very little metamorphic retrogression. Hence, a crustal section from unmetamorphosed indurated protolith (100°C, 1 kbar) to amphibolite-grade rocks (650°C, 7–10 kbar) is exposed. Although exposure occurred at different times, uplift along the Alpine Fault has resulted in the unroofing of the same deep crustal rocks that form the metamorphic basement of the Otago Schist, and consequently the Otago and Alpine schists can be considered as a single lithologic unit (Roser & Cooper 1990).

Quartz ± carbonate veins are common throughout the Otago and Alpine schists, some of which are mineralized with gold (Fig. 1). The gold-bearing quartz vein deposits are structurally hosted, and occur almost exclusively within greenschist-facies rocks. The largest deposit occurs at Macraes Flat in eastern Otago and produces ~3 tonnes of gold per annum at average grades of 1.6 g Au/tonne, with a total resource exceeding 125 tonnes Au (Craw 2002). Mineralization at Macraes occurred between 160 and 140 Ma, under lower greenschist facies conditions (300–350°C) in the brittle–ductile transition, as the rocks underwent uplift (McKeag *et al.* 1989, Teagle *et al.* 1990, Adams & Graham 1997). In addition to Au, the lodes are enriched in Ag, As, Sb, Se, Hg, W, Mo, Cr, Bi, C and S (McKeag *et al.* 1989, Craw *et al.* 1999, Craw 2002, Pitcairn 2004, Pitcairn *et al.* 2003, 2006a).

#### SAMPLING AND ANALYTICAL METHODS

A suite of samples representative of the variety of lithologies and metamorphic grades was collected across the Otago and Alpine schists (Fig. 1). Sampling locations, grid references, and metamorphic grade of individual samples are shown in Table 2, and sampling locations are also shown on Figure 1. Detailed thermobarometry has not been systematically carried out on these samples, and average metamorphic temperatures are taken from regional research (Mortimer 2000).

The mineralogy and textural associations were examined using reflected and transmitted light microscopy, and a representative set of samples was selected for investigation of mineral compositions. Sulfide abundances were obtained through automated thin section scanning on the Philips XL-30-ESEM with an INCA EDX detector at Stockholm University. The scanning was carried out using the gunshot-resolution (GSR) setting on the INCA feature-detection software,

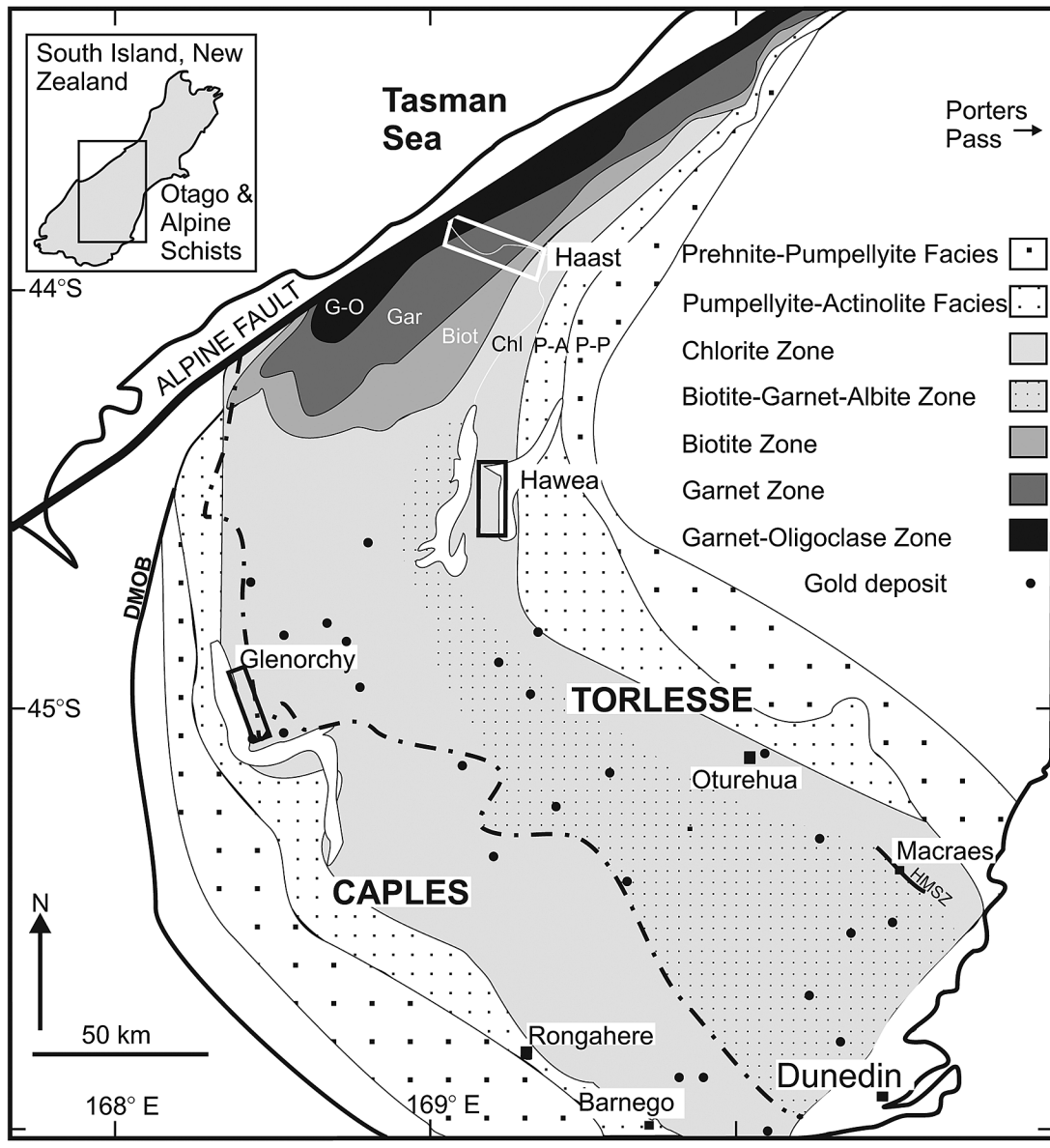


FIG. 1. Geological map of the Otago and Alpine schists, South Island, New Zealand, showing the Caples and Torlesse terranes, metamorphic isograds, sample localities (squares or boxes), gold deposits (black dots), and the Alpine Fault – Austro-Pacific plate contact. Abbreviations: HMSZ: Hyde Macraes Shear Zone, DMOB: Dun Mountain Ophiolite Belt.

which was programmed to apply grayscale variability in back-scattered detector SEM images to distinguish among different minerals. Results were calibrated with manual point-counts on the SEM, where every sulfide mineral in a set area was counted, analyzed and had its surface area measured. The same area of the thin section was scanned using the INCA feature-detection

software, and errors compared to manual point-counts are  $\pm 10\%$ . Total sulfide abundances estimated from the SEM scanning correlate favorably with S concentrations from whole-rock analysis, with an  $R^2$  of 0.57 (Fig. 2a).

Chemical analyses of sulfide minerals were carried out using the JEOL JXA 8900 electron microprobe at McGill University, equipped with five wavelength-

dispersion spectrometers and a Johansson-type crystal, which improves the peak : background ratio, allowing low detection-limits for Au (70 ppm; Almeida *et al.* 2010). Table 3 lists the elements sought, standards used (natural and synthetic minerals, alloys and pure metals), analytical lines, peak-counting times, and minimum detection-limits. The operating conditions in all cases were: acceleration voltage 20 kV, beam current 50 nA, a tightly focused beam (spot size around 1 µm),

and a long time counting (around 30 minutes for each analysis) owing to the low concentration of the trace elements sought. A beam current of 50 nA and long count-times were necessary for lower detection-limits. Continual analysis of the same spot in chalcopyrite showed no decrease of Cu and S intensities after 25 minutes, indicating that the high current and long count-times were not causing obvious damage to the sulfides. Similar tests were applied to other sulfide minerals, and no obvious damage was observed.

To ensure accurate measurements of trace concentrations, background and peak positions were chosen using spectra from synthetic minerals and actual X-ray spectra collected over long count-times on natural pyrite. This allowed selection of background-measurement positions that are free of interference from other X-ray peaks, which was especially important for Au and Hg. Silicon, Ti, and Ca were also measured as part of each analysis to identify possible contamination from the rock matrix. All possible X-ray line interferences were carefully checked, and in the case of interferences such as between Mo and Pb, different X-ray lines were used, and the Pulse Height Analyzer (PHA) adjusted to eliminate low-energy noise and the X-ray energies of interfering elements. Where possible, standards were matrix-matched to the minerals analyzed. For example, PbS was used for galena analyses (for S and Pb) in order to help reduce  $PbM\alpha$  and  $SK\alpha$  line interference. The raw data were corrected using a standard ZAF correction procedure. The detection limits were calculated as the minimum concentration required to produce count rates three times higher than the square root of the background ( $3\sigma$ ; 99% degree of confidence on the lowest detection-limit). Detection limits vary depending on the mineral being analyzed and also between individual analyses because of differences in sample matrix. Detection limits quoted are the highest individual value per element in each mineral analyzed. The range of detection limits for each element in different minerals is listed in Table 3.

Whole-rock analytical methods are described in greater detail in Pitcairn *et al.* (2006a). Arsenic, Hg, Sb, and Se whole-rock values were acquired using cold-vapor and hydride-generation atomic fluorescence spectroscopy at the National Oceanography Centre, Southampton, U.K., which allowed low limits of detection, <0.1 ppb. The samples were analyzed for gold at the National Oceanography Centre, Southampton, using a method for ultra-trace-level analysis of rocks for Au that involves chromatographic separation of Au from the sample matrix and analysis by ICP-MS. This approach yielded a detection limit of 0.01 ppb (Pitcairn *et al.* 2006b). The remaining major- and trace-element analyses were carried out using XRF and a LECO-C-S analyzer at the University of Leicester, U.K. (Pitcairn *et al.* 2006a).

TABLE 1. OCCURRENCE OF SILICATE, OXIDE AND HYDROXIDE, AND SULFIDE MINERALS OF OTAGO AND ALPINE SCHISTS, NEW ZEALAND

Grade	Unmeta-morphosed	Subgreen-schist	Greenschist	Amphibolite
Silicate, oxide, and hydroxide minerals				
Quartz	++++	++++	++++	++++
Plagioclase	++++	++++	++++	+++
K-feldspar	++	+		+
Muscovite	+	+++	++++	+++
Biotite	++	+	++	+++
Chlorite	+	+++	++++	
Epidote	+	++	+++	
Garnet	+		+	++
Titanite	++	++	++	+
OM	++	++	++	++
Calcite	+	+	+	+
Apatite	+	+	+	+
Zircon	+	+	+	+
Illite	+			
Pyroxene	+			
Zircon	+	+	+	+
Hornblende	+	+		+
Prehnite				
Pumpellyite				
Actinolite	+		++	
Stilpnomelane	+		+	
Tourmaline			+	+
Barite	+	+		
Magnetite	+	+		
Ilmenite	+	+	+	++
Rutile	+	+	+	
Goethite	+	+	+	+
Sulfide minerals (%)				
Pyrite	Mean 0.03 Range 0.001 to 0.1	0.008 0 to 0.04	0.026 0 to 0.15	0 0
Pyrrhotite	Mean 0 Range 0	0.034 0 to 0.2	0.017 0 to 0.4	0.08 0.4 to 0.16
Chalcopyrite	Mean 0.001 Range 0.0002 to 0.03	0.004 0.0004 to 0.01	0.001 0.000006 to 0.02	0.003 0.0002 to 0.005
Sphalerite	Mean 0.0007 Range 0 to 0.003	0.001 0.000008 to 0.02	0.0006 0.000006 to 0.003	0.00006 0 to 0.00001
Galena	Mean 0.0002 Range 0.000003 to 0.001	0.0002 0.000002 to 0.001	0.0001 0.000006 to 0.0007	0.00007 0 to 0.0002
Cobaltite	Mean 0.0002 Range 0 to 0.001	0.0006 0.000008 to 0.001	0.0001 0 to 0.0005	0 0

Crosses indicate relative proportions of silicate, oxide and hydroxide minerals. The abundances of sulfide minerals are reported as mean volume % values at each metamorphic grade, with the range of values also listed. Abundances were calculated from samples and data listed in Table 2. Abbreviation: OM: organic matter.

TABLE 2. SAMPLE NAMES, LOCALITIES, GRID REFERENCES, LITHOLOGIES, METAMORPHIC GRADES, SELECTED WHOLE-ROCK COMPOSITIONS, AND SULFIDE ABUNDANCES (%)

Sample Locality	C46 Porters Pass	C48 Porters Pass	C47 Porters Pass	C5 Barnego	A6 Barnego	A1 Otorehua	A3 Otorehua	A4 Rongahere	A5 Rongahere	A60 Hawea	A63 Hawea
GR	E 2409656 N 5766383	E 2409656 N 5766383	E 2409656 N 5766383	259437 (17) GW Un-met 100	259437 (17) GW Un-met 100	265582 (15) Psam. Sub-GS 200	265582 (15) Pel. Sub-GS 200	237463 (17) Pel. Sub-GS 200	237463 (17) Pel. Sub-GS 200	213626 (14) Psam. Sub-GS 200	213626 (14) Psam. Sub-GS 200
Lithology	GW	GW	GW								
Met. grade	Un-met	Un-met	Un-met								
Temp. (°C)	100	100	100								
Fe <sub>2</sub> O <sub>3</sub> wt.%	4.5	4.4	4.6	6.7	6.9	3.8	6.4	4.4	4.2	4.1	4.7
S	0.02	0.03	0.03	0.04	0.08	0.01	0.06	0.02	0.03	0.01	0.02
Co ppm	11.0	n.a.	9.6	17.0	19.1	8.2	14.5	8.6	7.9	8.7	10.5
Ni	12.5	n.a.	18.1	23.6	23.8	8.1	26.5	9.3	2.6	5.1	13.6
Cu	9.5	9.9	14.3	24.9	27.1	b.d.	21.3	9.7	b.d.	0.6	14.0
Zn	64.7	59.9	63.5	78.6	81.1	44.5	100.1	57.4	43.6	49.9	66.0
As	3.87	2.89	3.59	2.41	8.53	4.18	31.27	2.95	7.33	9.37	5.12
Se	n.a.	0.03	0.004	0.05	0.12	n.a.	n.a.	0.06	n.a.	n.a.	0.07
Mo	n.a.	n.a.	0.84	0.89	0.72	n.a.	n.a.	0.70	n.a.	n.a.	0.51
Ag	n.a.	n.a.	b.d.	0.05	b.d.	n.a.	n.a.	b.d.	n.a.	n.a.	0.11
Sb	0.24	0.21	0.22	0.31	0.24	0.44	0.70	0.23	0.49	1.05	0.62
Au ppb	0.38	0.49	0.54	0.83	0.74	0.70	1.70	6.98	0.34	0.29	0.34
Hg ppm	0.064	0.065	0.082	0.075	0.105	0.017	0.051	0.052	0.031	0.026	0.036
Pb	26.0	19.0	19.9	3.6	9.6	19.3	28.9	11.3	14.3	18.4	14.8
Sulfide abundance from SEM scanning (modal %)											
Total S	0.044	0.01	0.0028	0.002	0.109	0.024	0.01	0.006	0.081	0.02	0.014
Pyrite	0.042	0.007	0.0026	0.001	0.103	0.004	0.007	0.01	0.04	0	0.0014
Pyrrhotite	0	0	0	0	0	0.012	0	0.0001	0.026	0.016	0.0125
Sphalerite	0.000005	0.003	0.00003	0	0.0005	0.002	0.002	0.002	0.0024	0.001	0.00008
Chalcopyrite	0.002	0.0004	0.0002	0.001	0.003	0.005	0.0007	0.0004	0.013	0.004	0.0005
Galena	0.00003	0.00005	0.00005	0.000003	0.001	0.0005	0.000002	0.001	0.00014	0.0003	0.000002
Cobaltite	0	0	0.000003	0	0.001	0.0004	0.0002	0.001	0.0005	0.001	0.000008

## ABUNDANCE, TEXTURE AND CHEMICAL COMPOSITION OF SULFIDE MINERALS

### Unmetamorphosed samples

Unmetamorphosed samples used in this study are greywackes from both the Torlesse and Caples terranes (Fig. 1). The greywackes contain quartz, plagioclase, K-feldspar, lithic fragments, chlorite, biotite, augite, illite, titanite, magnetite, ilmenite, rutile, organic matter ± muscovite, epidote, garnet, barite, and hornblende (Table 1). Greywackes from the Caples Terrane have higher proportions of lithic fragments, detrital pyroxene and hornblende than rocks of the Torlesse Terrane.

Pyrite is the most common sulfide mineral in the unmetamorphosed rocks (Table 1, Fig. 2D). It occurs mainly as spherical aggregates of small grains, commonly forming a frambooidal texture (Fig. 3). These aggregates are commonly porous and contain micro-inclusions of chalcopyrite, sphalerite, galena and cobaltite. They occur in the matrix of the rock, associated with organic matter, altered detrital plagioclase, quartz and biotite (Figs. 3A–3C). Spherical pyrite commonly exhibits concentric zones in back-scattered

electron images, indicating compositional variation (Figs. 3A, C). Chalcopyrite, sphalerite, galena, and rare pyrite occur as isolated grains with a subhedral to euhedral shape (Fig. 3F). Locally porous spherical pyrite overgrows relict subhedral pyrite that is interpreted to be detrital in origin (Fig. 3E).

Spherical pyrite contains the greatest number and highest concentrations of minor elements of the sulfide minerals identified in the unmetamorphosed rocks. Average concentrations of As, Co, Cu, and Ni are significantly above detection limits, ranging up to 13900 ppm (Table 4). Silver, Au, Hg, Mo, Sb, W, and Zn are above detection in some individual minerals, but average concentrations of these elements are below the limits of detection (Table 4). The minor elements are heterogeneously distributed within the spherical pyrite. For example, As has average concentrations of 3190 ppm, but the concentrations range from below the detection limit (120 ppm) to 13800 ppm (Table 4). An X-ray elemental map of a cluster of spherical grains of pyrite from an unmetamorphosed greywacke from the Caples Terrane shows the spatial distribution of selected minor elements (Fig. 4). Arsenic and Co are enriched in concentric zones around the rims of the grains, and

TABLE 2 (cont'd). SAMPLE NAMES, LOCALITIES, GRID REFERENCES, LITHOLOGIES, METAMORPHIC GRADES, SELECTED WHOLE-ROCK COMPOSITIONS, AND SULFIDE ABUNDANCES (%)

Sample Locality	A64 Hawea	A67 Hawea	B84 Glenorchy	A84 Hawea	B2 Hawea	B36 Hawea	C72 Haast	C61 Haast	C76 Haast	C56 Haast	C59 Haast
Lithology	GR 213626 (14)	213626 (14)	500705 (E41)	21126312 (14)	20906320 (14)	20706340 (14)	197813 (G37)	153881 (G37)	009888 (F37)	009888 (F37)	009888 (F37)
Met. grade	Sub-GS	Sub-GS	Sub-GS	GS	GS	GS	GS	Amph.	Amph.	Amph.	Amph.
Temp. (°C)	200	200	200	350	350	350	350	575	575	575	575
Fe <sub>2</sub> O <sub>3</sub> wt. %	3.3	3.4	6.3	4.8	4.0	4.3	4.4	8.4	5.2	4.4	3.9
S	0.01	0.02	0.12	0.02	0.11	0.01	0.01	0.02	0.09	0.07	0.04
Co ppm	7.2	5.9	16.3	n.a.	7.9	n.a.	8.8	20.8	n.a.	8.7	8.0
Ni	10.0	7.3	19.5	n.a.	13.8	n.a.	9.5	49.0	n.a.	11.1	9.9
Cu	8.7	b.d.	25.2	11.6	20.0	9.0	9.7	8.5	10.6	14.2	8.8
Zn	50.9	42.1	79.8	63.2	57.0	60.3	56.6	124.5	74.8	71.7	63.2
As	6.94	8.07	7.78	6.92	2.65	6.71	5.53	0.54	0.10	0.55	0.06
Se	0.12	n.a.	0.15	0.14	0.22	0.135	0.04	0.015	0.02	0.03	0.07
Mo	2.08	n.a.	1.12	n.a.	0.53	n.a.	0.25	0.62	n.a.	0.74	0.51
Ag	0.06	n.a.	0.07	n.a.	0.11	n.a.	0.04	b.d.	n.a.	b.d.	b.d.
Sb	0.40	0.15	0.55	1.05	0.64	0.28	0.19	0.09	0.04	0.002	0.002
Au ppb	0.22	0.23	0.51	0.17	1.31	0.22	0.31	0.18	0.11	0.17	0.25
Hg ppm	0.043	0.006	0.014	0.014	0.004	0.009	0.006	0.003	0.003	0.003	0.002
Pb	15.9	12.4	22.8	18.5	24.9	13.9	17.2	24.9	18.5	24.6	19.5
Sulfide abundance from SEM scanning (modal %)											
Total S	0.009	0.014	0.22	0.018	0.16	0.016	0.013	0.005	0.069	0.048	0.16
Pyrite	0.0007	0	0	0.001	0.155	0	0	0	0	0	0
Pyrrhotite	0.006	0.013	0.2	0.014	0	0.015	0.011	0.005	0.065	0.043	0.156
Sphalerite	0.0007	0.0005	0.0002	0.0002	0.003	0.00009	0.000008	0.000001	0	0.000004	0.00001
Chalcopyrite	0.0005	0.000004	0.01	0.002	0.001	0.001	0.002	0.00002	0.004	0.005	0.004
Galena	0.00005	0.00009	0.0001	0.00006	0.000003	0.00007	0.00002	0.00002	0	0.00003	0.00006
Cobaltite	0.0004	0.0002	0.001	0.00009	0.0005	0.0001	0	0	0	0	0

Grid References show easting or northing or 6-figure reference and map sheet number in brackets. Abbreviations: GW: greywacke, Psam: psammites, Pel: pelite, QFS: quartzofeldspathic, Un-met: unmetamorphosed, Sub-GS: subgreenschist, GS: greenschist, Amph: amphibolite, b.d.: below detection, n.a.: not analyzed.

in discrete spots within the grain, most likely related to small inclusions of cobaltite (Fig. 4).

Chalcopyrite generally contains fewer minor elements than spherical pyrite, although Ag, As, Hg, and Se concentrations are above detection limits in a few individual grains (Table 5). Sphalerite, besides being the major host of Zn, also contains average concentrations of Co and Cu that are above their relative limits of detection (Table 6). Galena contains average concentrations of Cu and Se above detection, and Hg and Sb concentrations above detection in individual analyses (Table 7). Cobaltite occurs as small inclusions in aggregates of spherical pyrite, but the grain size is too small for quantitative analysis.

#### Subgreenschist-facies samples

Subgreenschist-facies samples contain small proportions of detrital minerals such as K-feldspar, muscovite, biotite, epidote, magnetite, rutile, and ilmenite, but are mainly composed of authigenic minerals such as quartz, albite, prehnite, pumpellyite, chlorite, muscovite, titanite, epidote, and actinolite (Bishop 1972;

Table 1). Pumpellyite grows at the expense of prehnite and detrital chlorite, muscovite and actinolite appear to grow through the breakdown of detrital K-feldspar and amphibole, respectively, and titanite partially replaces detrital ilmenite (Table 1). Two of the nine subgreenschist-facies samples contain barite, but in all other samples, the sulfides are the only identified S-bearing mineral. Some of the subgreenschist-facies samples preserve detrital textures and have higher proportions of detrital minerals, whereas the majority display a penetrative cleavage and development of segregation lamellae of quartz + albite.

Two distinct changes occur in the sulfide mineral assemblage in subgreenschist-facies rocks. Pyrrhotite becomes the most abundant sulfide (Figs. 2C to 2I), and the most common textural association changes from spherical pyrite grains to irregularly shaped composite grains of pyrite or pyrrhotite with subordinate chalcopyrite, sphalerite, galena and cobaltite (Fig. 5). Spherical pyrite occurs in samples where the detrital sedimentary textures are preserved (*e.g.*, sample A4; Table 2), but it is much less abundant than in unmetamorphosed rocks (Fig. 2). Pyrite also occurs in composite grains of

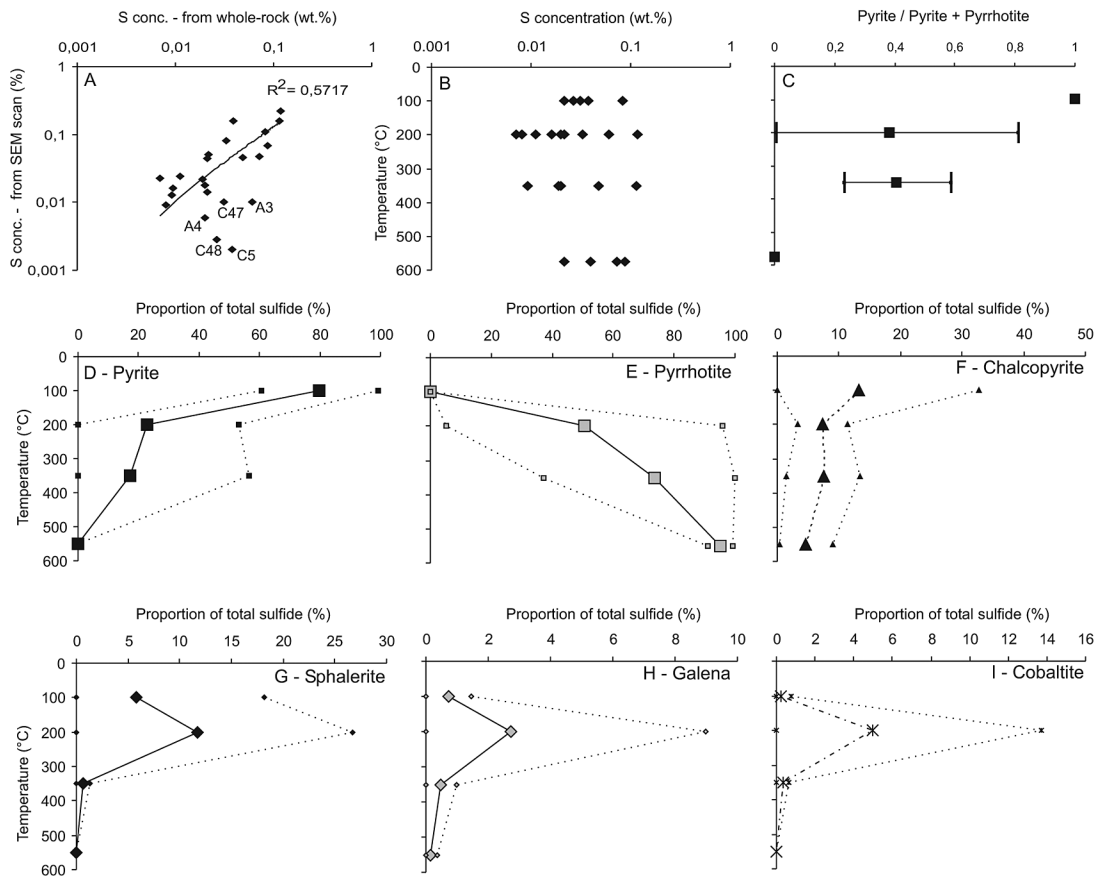


FIG. 2. A. Plot of S concentration estimated from total sulfide abundance from SEM scans *versus* S concentration measured in whole-rock samples. The correlation coefficient ( $R^2$ ) is equal to 0.57. The labeled outliers contain barite ( $\text{BaSO}_4$ ). B. Plot of whole-rock S concentration (wt.%) *versus* metamorphic grade. C. The proportion of pyrite and pyrrhotite at different metamorphic temperatures. The horizontal bars represent one standard deviation. D to I. The proportion of pyrite, pyrrhotite, chalcopyrite, sphalerite, galena and cobaltite relative to total sulfide at each metamorphic grade. Dashed lines represent one standard deviation. Values are shown in Tables 1 and 2.

FIG. 3. Back-scattered electron images (BSE) and reflected light microphotographs (RL) of sulfide grains from unmetamorphosed samples of the Torlesse and Caples terrane. Minerals are labeled and positions of electron-microprobe analyses are shown with trace-element concentrations listed at the side. A, B and C. Sample C48 showing aggregates of spherical pyrite composed of framboidal grains overgrown by concentric zones. There is a compositional difference between the core and rim of many grains, shown by darker and brighter colors (BSE). D. Sample A6 showing a composite grain of pyrite containing inclusions of cobaltite, sphalerite and chalcopyrite mainly in the outer concentric zones surrounding framboidal-textured cores (BSE). E. Sample A6 showing a porous composite outer layer of pyrite that contains inclusions of chalcopyrite and cobaltite, attached to a subhedral, homogeneous grain of pyrite (BSE). F. Sample C5 with euhedral grains of pyrite (RL). Results of analyses: 1) 6900 ppm As, 1100 ppm Co, 410 ppm Ni, 2) 12000 ppm As, 1100 ppm Co, 200 ppm Sb, 3) 600 ppm As, 900 ppm Co, 5) 2900 ppm As, 1600 ppm Co, 640 ppm Ni, 5) 4400 ppm As, 2700 ppm Co, 1100 ppm Ni, 6) 1100 ppm Co, 510 ppm Ni, 110 ppm As, 7) 8600 ppm Co, 3000 ppm Ni, 2800 ppm As, 500 ppm Sb, 240 ppm Ag, 8) no trace elements detected, 9) 1350 ppm Co, 770 ppm As, 390 ppm Ni, 10) no trace elements detected. Mineral symbols (same for all figures): Bt: biotite, Cbt: cobaltite, Cc: calcite, Ccp: chalcopyrite, Chl: chlorite, Ep: epidote, Gn: galena, Gt: goethite, Ilm: ilmenite, Ms: muscovite, Pl: plagioclase, Po: pyrrhotite, Py: pyrite, Qtz: quartz, Sp: sphalerite, Ttn: titanite, Ull: ullmannite.

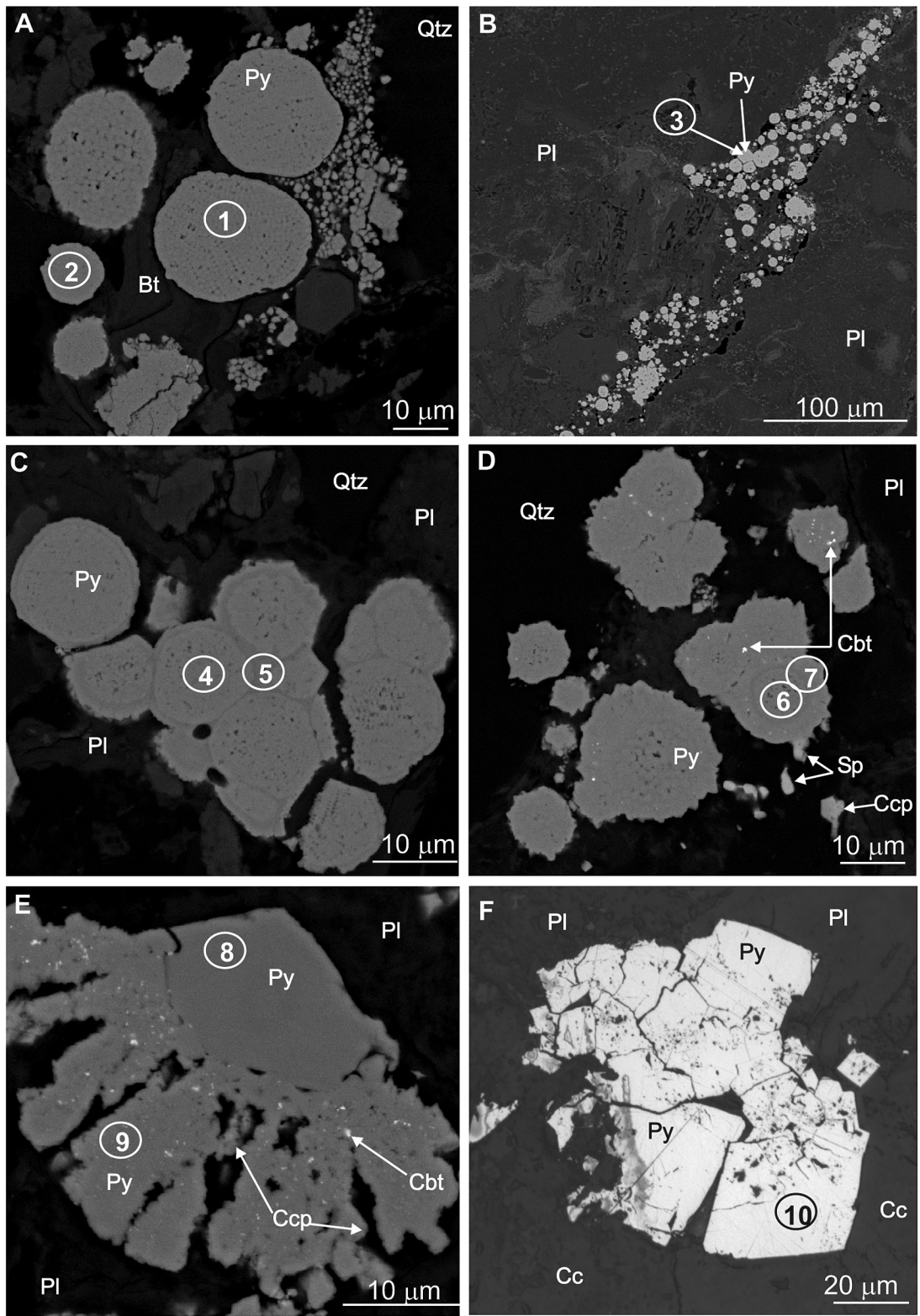


TABLE 3. CONDITIONS OF ANALYSIS\* OF SULFIDE MINERALS

	Standard	X-ray line	Channel	Crystal	Peak count-time (s)	Detection limits range (ppm)
Ag	Au <sub>60</sub> Ag <sub>40</sub>	L $\alpha$	1	PETJ	150	230 – 340
As	Canmet CoNiAs	L $\beta$	2	TAP	400	110 – 270
Au	Au <sub>60</sub> Ag <sub>40</sub>	M $\alpha$	5	PETH	540	70 – 100
Ca	Diopside	K $\alpha$	4	PETJ	50	80 – 110
Co	Canmet CoNiAs	K $\alpha$	3	LIF	40	180 – 250
Cu	Canmet chalcopyrite	K $\alpha$	3	LIF	100	120 – 220
Fe	Canmet pyrite	K $\alpha$	3	LIF	20	360 – 520
Hg	HgS	L $\alpha$	3	LIF	340	360 – 600
Mo	Canmet CaMoO <sub>4</sub>	L $\beta$	1	PETJ	120	260 – 1100
Ni	Canmet pentlandite	K $\alpha$	3	LIF	80	150 – 270
Pb	Canmet PbS	M $\alpha$	5	PETH	150	220 – 960
S	Canmet pyrite	K $\alpha$	5	PETH	10	110 – 240
Sb	Canmet stibnite	L $\alpha$	4	PETJ	340	80 – 100
Se	Se	L $\alpha$	2	PETJ	40	100 – 170
Si	Diopside	K $\alpha$	2	TAP	20	100 – 150
Ti	TiO <sub>2</sub>	K $\alpha$	4	PETJ	60	180 – 220
W	W metal	M $\alpha$	1	PETJ	400	110 – 360
Zn	Canmet ZnS	L $\alpha$	2	TAP	40	220 – 900

\* Wavelength-dispersion electron-microprobe analysis.

irregular texture with subordinate chalcopyrite, sphalerite, galena, and cobaltite (Figs. 5a, 5b). The majority of subgreenschist-facies rocks (*e.g.*, samples A63, A64, B84; Table 2) show the development of a foliation, and pyrrhotite is much more abundant than pyrite in these rocks, occurring in composite grains with chalcopyrite, sphalerite, galena and cobaltite (Figs. 5C to 5G), and as isolated grains. Pyrite and pyrrhotite occur together in some samples, and locally within the same grains in which pyrrhotite replaces pyrite along preferential crystallographic planes (*e.g.*, Fig. 6F). The variable degree of replacement of pyrite by pyrrhotite is highlighted by the large range in the pyrite/(pyrite + pyrrhotite) values shown in Figure 2B.

Abundances of cobaltite and, to a lesser degree, galena dramatically increase in subgreenschist-facies rocks compared to unmetamorphosed rocks (Fig. 2I). Pyrite, pyrrhotite, chalcopyrite, sphalerite, galena, and cobaltite also occur as isolated grains that commonly truncate the metamorphic foliation, suggesting that at least the outer zones of these grains formed synkinematically with formation of the main foliation. In samples where there is a strong foliation, sulfides are commonly elongate parallel to it (Fig. 5G). Pentlandite and ullmannite (NiSbS) have also been identified. Ullmannite is a rare constituent of pyrrhotite composites (Fig. 5E), and pentlandite occurs as tabular inclusions within pyrrhotite. Pyrrhotite is locally replaced by goethite along grain boundaries and certain crystallographic planes (Figs. 6B, 6D and 6E).

In spherical pyrite from the subgreenschist-facies rocks, the concentrations of minor elements are similar to those in spherical pyrite from unmetamorphosed rocks, although Sb concentrations are higher, with

average values of  $590 \pm 330$  ppm (Table 4). Composite pyrite also contains abundant minor elements, although generally at lower concentrations than in spherical pyrite, and average concentrations As, Co, Cu, Ni, and Sb are above limits of detection (Table 4). An X-ray elemental map of a composite grain of pyrite in a subgreenschist-facies sample from the Caples Terrane shows the heterogeneous distribution of minor elements (Fig. 7). The bright spots related to high As and Co concentrations are most likely due to small grains of cobaltite, but As is also enriched around the rim of that composite grain, and within some of the sphalerite inclusions. Isolated pyrite has different trace-element contents from the spherical and composite pyrite. Such grains commonly contain no detectable As or Cu, but contain significant average concentrations of Co, Ni, Sb, and in individual samples, W (Table 4).

Pyrrhotite contains abundant Co ( $1110 \pm 490$  ppm) and Ni ( $3970 \pm 2540$  ppm), but average values of Ag, As, Au, Cu, Hg, Sb, Se, W, and Zn are below the limits of detection (Table 8). Chalcopyrite contains none of the minor elements sought at detectable levels (Table 5). Sphalerite contains average values of Co, Cu, and Hg above detection, and Ag, As, and W in some individual cases (Table 6). In subgreenschist-facies rocks, galena predominantly occurs as composite grains, and it contains average concentrations above the detection limits for Au, Ag, Co, Cu, Hg, Se and Sb (Table 7). Cobaltite is a major host of As and Co in subgreenschist-facies samples, and it contains significant average concentrations of Ni, Sb, Mo, and Au in individual grains (Table 9). The single grain of ullmannite (NiSbS) found in a subgreenschist-facies sample (Fig. 5E) contains detectable minor As, Co, Hg, and Se (Table 9).

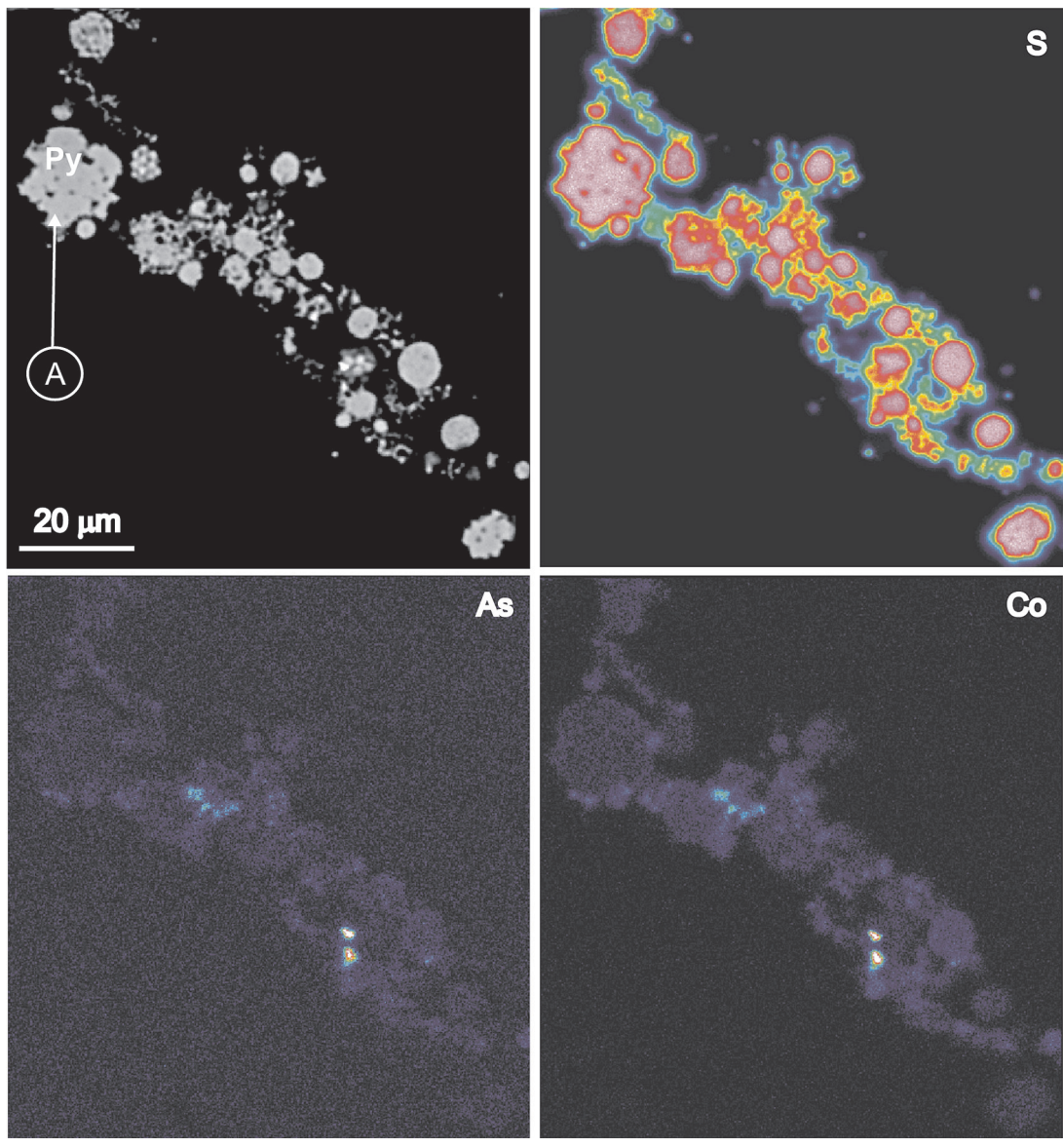


FIG. 4. A BSE and X-ray elemental map for S, As, and Co in spherical pyrite from sample A6. The brighter colors represent higher concentrations. Arsenic and Co are enriched along the rim of spherical crystals of pyrite, and the very bright Co and As patches represent small inclusions of cobaltite. The site of a WDS analysis in the pyrite rim that yielded 500 ppm Co, and 460 ppm As is shown as "A" in the BSE image.

#### *Greenschist-facies samples*

Greenschist-facies rocks comprise quartz, albite, chlorite, muscovite, actinolite, epidote, titanite  $\pm$  stilpnomelane, biotite, and garnet (Table 1). Greenschist-facies samples are almost wholly recrystallized, with common segregation lamellae of quartz + feldspar, and

actinolite + epidote + chlorite + muscovite. Actinolite and epidote seem to grow at the expense of pumpellyite and chlorite, and this is supported by modal decreases in chlorite and increases in actinolite and epidote at the pumpellyite-out isograd (Bishop 1972). Biotite and garnet are common in upper-greenschist-facies samples, and ilmenite is strongly altered to titanite (Table 1).

In greenschist-facies samples, the relative abundance of pyrite, sphalerite, galena and cobaltite decrease (Figs. 2D to 2G, 2H, and 2I). Commensurately, the relative abundance of pyrrhotite increases (Fig. 2E). All sulfides in greenschist-facies samples show regular synkinematic textures in which the outer zones of the sulfide grains truncate the foliation (Figs. 8A to 8D), and the irregular, composite grains that were common in subgreenschist-facies samples do not occur. Cobaltite commonly occurs as inclusions in pyrrhotite or as small crystals proximal to or attached to pyrrhotite

grain-boundaries (Fig. 8A). Chalcopyrite, sphalerite and galena also commonly occur proximal to pyrrhotite, perhaps because of the breakdown of composite grains with increasing metamorphic recrystallization. Few greenschist-facies samples contain pyrite, but where it occurs, it can be abundant (e.g., sample B2, Table 3), and is commonly euhedral (Fig. 8C). Post-metamorphic oxidation of pyrrhotite to goethite occurs in some samples of Otago Schist, but more commonly in samples of Alpine Schist (Figs. 8B and 8D).

TABLE 4. CHEMICAL COMPOSITION OF PYRITE FROM THE OTAGO AND ALPINE SCHISTS, NEW ZEALAND,  
RANKED ACCORDING TO METAMORPHIC GRADE

N		Ag	As	Au	Co	Cu	Fe	Hg	Mo	Ni	Pb	S	Sb	Se	Si	W	Zn	Total	
<b>Spherical</b>																			
26	All	Mean	b.d.	0.316	b.d.	0.144	0.155	45.1	b.d.	0.051	b.d.	51.5	b.d.	b.d.	0.115	b.d.	b.d.	97.5	
		SD		0.403		0.113	0.331	0.8		0.031		0.9		0.139				1.3	
		Max		0.027	1.384	0.009	0.398	1.391	46.6	0.035	b.d.	0.108	b.d.	53.2	0.082	0.015	0.531	b.d.	0.040 100.0
		Min		b.d.	b.d.	b.d.	b.d.	44.1	b.d.	95.2									
24	Un-met	Mean	b.d.	0.324	b.d.	0.136	0.165	45.1	b.d.	b.d.	0.050	b.d.	51.5	b.d.	b.d.	0.101	b.d.	b.d.	97.4
(100)		SD		0.419		0.113	0.343	0.8		0.031		0.9		0.134					1.3
		Max		0.027	1.384	0.009	0.398	1.391	46.6	b.d.	b.d.	0.108	b.d.	53.2	0.024	0.015	0.531	b.d.	0.040 100.0
		Min		b.d.	b.d.	b.d.	b.d.	44.1	b.d.	95.2									
2	Sub	Mean	b.d.	0.227	b.d.	0.233	0.030	44.7	b.d.	b.d.	0.056	b.d.	52.3	0.059	b.d.	0.287	b.d.	b.d.	98.0
GS		SD		0.122		0.093	0.009	0.8			0.040		0.6	0.033		0.099			1.1
(200)		Max		0.313	b.d.	0.298	0.036	45.3	0.035	b.d.	0.084	b.d.	52.7	0.082	b.d.	0.357	b.d.	b.d.	98.8
		Min		b.d.	0.141	b.d.	0.167	0.023	44.1	b.d.	b.d.	0.027	b.d.	51.9	0.036	b.d.	0.217	b.d.	97.2
<b>Composite</b>																			
15	Sub	Mean	b.d.	0.129	b.d.	0.121	0.041	45.1	b.d.	b.d.	0.045	b.d.	52.3	0.022	b.d.	0.161	b.d.	0.119	98.1
GS		SD		0.245		0.167	0.057	1.1			0.052		0.9	0.037		0.286		0.327	1.1
(200)		Max		0.023	0.897	0.010	0.473	0.226	46.3	0.037	b.d.	0.142	b.d.	53.2	0.124	0.011	1.014	b.d.	1.242 99.7
		Min		b.d.	b.d.	b.d.	b.d.	42.8	b.d.	96.1									
<b>Regular</b>																			
38	All	Mean	b.d.	0.026	b.d.	0.153	0.027	46.0	b.d.	b.d.	0.340	b.d.	52.8	0.077	b.d.	0.053	b.d.	b.d.	99.5
		SD		0.059		0.292	0.069	1.2			0.608		0.5	0.156		0.082			0.8
		Max		b.d.	0.312	0.011	0.090	0.371	47.6	0.035	0.057	2.487	b.d.	53.4	0.699	0.038	0.370	b.d.	0.038 100.8
		Min		b.d.	b.d.	b.d.	b.d.	42.6	b.d.	97.0									
15	Un-met	Mean	b.d.	0.016	b.d.	0.063	46.3	b.d.	b.d.	0.012		0.6		0.012	b.d.	0.072	b.d.	b.d.	99.6
(100)		SD		0.018		0.102	0.5									0.103			0.7
		Max		b.d.	0.059	b.d.	0.033	0.371	46.9	0.035	0.057	0.034	b.d.	53.4	b.d.	0.014	0.370	b.d.	0.038 100.3
		Min		b.d.	b.d.	b.d.	b.d.	45.4	b.d.	97.8									
10	Sub	Mean	b.d.	b.d.	b.d.	0.458	b.d.	44.5	b.d.	b.d.	0.945	b.d.	52.6	0.206	b.d.	0.030	b.d.	b.d.	98.9
GS		SD		0.368		1.0					0.788		0.3	0.153		0.032			0.7
(200)		Max		b.d.	0.022	b.d.	1.090	b.d.	46.0	b.d.	b.d.	2.487	b.d.	53.1	0.449	0.023	0.094	b.d.	0.036 99.6
		Min		b.d.	b.d.	b.d.	b.d.	42.6	b.d.	97.0									
13	GS	Mean	b.d.	0.054	b.d.	0.088	b.d.	46.8	b.d.	b.d.	0.137	b.d.	52.6	0.065	b.d.	b.d.	b.d.	b.d.	99.9
(350)		SD		0.095		0.227	0.9				0.288		0.5	0.191					0.7
		Max		b.d.	0.312	0.011	0.786	0.019	47.6	b.d.	0.027	0.802	b.d.	53.3	0.699	0.038	b.d.	b.d.	100.8
		Min		b.d.	b.d.	b.d.	b.d.	44.4	b.d.	98.4									
M.d.l.				0.023	0.012	0.008	0.018	0.015	0.0	0.035	0.026	0.017	0.038	0.0	0.008	0.010	0.010	0.031 0.027	

Concentrations from WDS electron-microprobe analysis are in weight %. Textural classifications are described in the text. Results that are below detection are not included in the calculation of mean values. Abbreviations: Un-met: unmetamorphosed, GS: greenschist, Amph: amphibolite, N: number of samples, SD: standard deviation ( $1\sigma$ ), Max and Min: maximum and minimum values, b.d.: below detection, M.d.l.: minimum detection limit. In parentheses, the approximate temperature of equilibration.

TABLE 5. CHEMICAL COMPOSITION OF CHALCOPYRITE FROM THE OTAGO AND ALPINE SCHISTS, NEW ZEALAND,  
RANKED ACCORDING TO METAMORPHIC GRADE

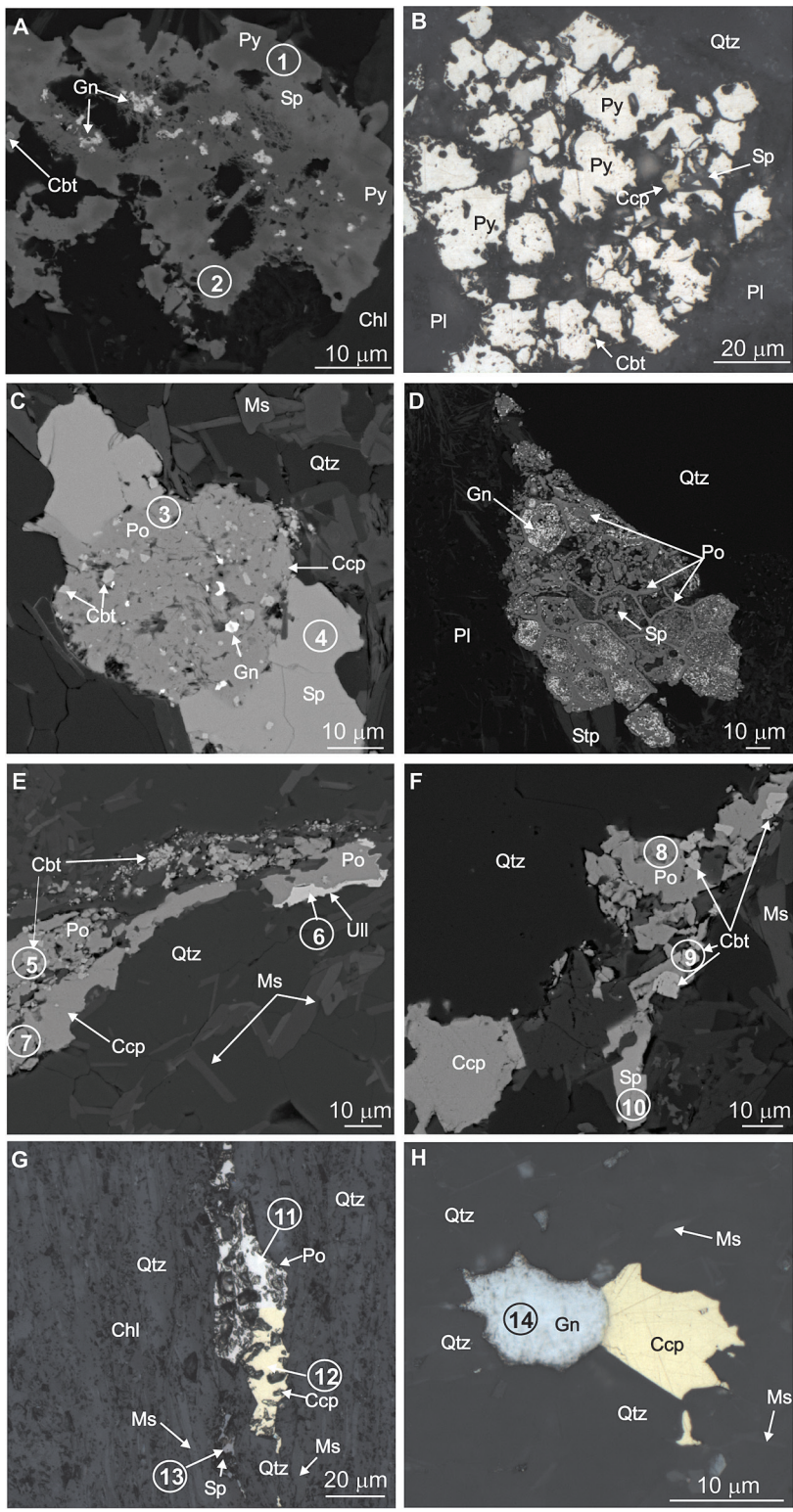
N		Ag	As	Au	Co	Cu	Fe	Hg	Mo	Ni	Pb	S	Sb	Se	Si	W	Zn	Total		
23	All	Mean	b.d.	b.d.	b.d.	33.5	30.2	b.d.	b.d.	b.d.	b.d.	34.9	b.d.	b.d.	0.192	b.d.	0.102	98.8		
		SD				1.7	0.7					0.8			0.313		0.227	1.3		
		Max	0.047	0.022	b.d.	b.d.	34.7	31.6	0.073	b.d.	0.015	b.d.	37.7	0.018	0.019	0.977	b.d.	0.740	100.9	
		Min	b.d.	b.d.	b.d.	26.0	28.7	b.d.	b.d.	b.d.	b.d.	33.5	b.d.	b.d.	b.d.	b.d.	b.d.	95.5		
4	Un-met	Mean	b.d.	b.d.	b.d.	b.d.	31.2	30.1	b.d.	b.d.	b.d.	b.d.	35.1	b.d.	b.d.	0.489	b.d.	b.d.	97.1	
	(100)	SD				3.5	1.1					1.8			0.461			1.4		
		Max	0.027	0.013	b.d.	b.d.	33.7	31.6	0.073	b.d.	b.d.	b.d.	37.7	b.d.	0.019	0.977	b.d.	b.d.	98.7	
		Min	b.d.	b.d.	b.d.	b.d.	26.0	29.1	b.d.	b.d.	b.d.	b.d.	33.5	b.d.	b.d.	0.021	b.d.	b.d.	95.5	
5	Sub	Mean	b.d.	b.d.	b.d.	b.d.	34.0	30.0	b.d.	b.d.	b.d.	b.d.	35.1	b.d.	b.d.	0.083	b.d.	b.d.	99.3	
	(GS)	SD				0.2	0.6					0.2			0.072			0.7		
		Max	b.d.	0.022	b.d.	b.d.	34.2	30.9	b.d.	b.d.	b.d.	b.d.	35.5	b.d.	b.d.	0.185	b.d.	b.d.	100.1	
		Min	b.d.	b.d.	b.d.	b.d.	33.8	29.4	b.d.	b.d.	b.d.	b.d.	34.9	b.d.	b.d.	b.d.	b.d.	b.d.	98.5	
12	GS	Mean	b.d.	b.d.	b.d.	b.d.	34.0	30.3	b.d.	b.d.	b.d.	b.d.	34.8	b.d.	b.d.	0.032	b.d.	0.108	99.3	
	(350)	SD				0.4	0.7					0.4			0.044			0.256	1.0	
		Max	0.047	b.d.	b.d.	b.d.	34.7	31.0	0.044	b.d.	b.d.	b.d.	35.3	0.013	0.015	0.098	b.d.	0.740	100.9	
		Min	b.d.	b.d.	b.d.	b.d.	33.6	28.7	b.d.	b.d.	b.d.	b.d.	34.0	b.d.	b.d.	b.d.	b.d.	b.d.	97.4	
2	Amph	Mean	b.d.	b.d.	b.d.	b.d.	33.4	30.6	b.d.	b.d.	b.d.	b.d.	34.3	0.010	b.d.	b.d.	b.d.	0.080	98.3	
	(575)	SD				0.7	0.6					0.1	0.013						0.054	1.3
		Max	b.d.	b.d.	b.d.	b.d.	33.8	31.0	b.d.	b.d.	0.015	b.d.	34.3	0.018	b.d.	b.d.	b.d.	0.118	99.2	
		Min	b.d.	b.d.	b.d.	b.d.	32.9	30.2	b.d.	b.d.	b.d.	b.d.	34.2	b.d.	b.d.	b.d.	b.d.	0.041	97.5	
M.d.l.			0.025	0.011	0.007	0.019	0.017	0.0	0.036	0.101	0.015	0.027	0.01	0.010	0.013	0.010	0.017	0.022		

Concentrations from WDS microprobe analyses are expressed in weight %. Results that are below detection are not included in the calculation of mean values. Abbreviations as Table 4. M.d.l.: minimum detection limit. In parentheses, the approximate temperature of equilibration.

TABLE 6. CHEMICAL COMPOSITION OF SPHALERITE FROM THE OTAGO AND ALPINE SCHISTS, NEW ZEALAND  
RANKED ACCORDING TO METAMORPHIC GRADE

N		Ag	As	Au	Co	Cu	Fe	Hg	Mo	Ni	Pb	S	Sb	Se	Si	W	Zn	Total	
13	All	Mean	b.d.	b.d.	b.d.	0.077	0.160	4.7	0.050	b.d.	b.d.	33.1	b.d.	b.d.	0.101	b.d.	62.6	100.9	
		SD				0.040	0.245	1.1	0.038			0.3			0.144		1.2	0.7	
		Max	0.027	0.026	b.d.	0.123	0.769	7.6	0.110	b.d.	0.025	b.d.	34.0	b.d.	0.013	0.456	0.032	63.8	102.0
		Min	b.d.	b.d.	b.d.	b.d.	b.d.	3.4	b.d.	b.d.	b.d.	b.d.	32.8	b.d.	b.d.	b.d.	b.d.	59.1	100.0
2	Un-met	Mean	b.d.	b.d.	b.d.	0.122	0.527	4.1	b.d.	b.d.	b.d.	b.d.	33.0	b.d.	b.d.	0.161	b.d.	62.5	100.5
	(100)	SD				0.343	0.2					0.1			0.139		0.2	0.3	
		Max	b.d.	b.d.	b.d.	0.123	0.769	4.2	b.d.	b.d.	b.d.	b.d.	33.1	b.d.	b.d.	0.259	b.d.	62.6	100.7
		Min	b.d.	b.d.	b.d.	0.121	0.284	3.9	b.d.	b.d.	b.d.	b.d.	32.9	b.d.	b.d.	0.063	b.d.	62.4	100.3
8	Sub	Mean	b.d.	b.d.	b.d.	0.083	0.056	4.5	0.072	b.d.	b.d.	b.d.	33.1	b.d.	b.d.	0.086	b.d.	63.1	101.1
	(GS)	SD				0.030	0.074	0.4	0.029				b.d.			0.151		0.5	0.7
		Max	0.027	0.026	b.d.	0.119	0.189	5.1	0.110	b.d.	0.025	b.d.	34.0	b.d.	0.011	0.456	0.032	63.8	102.0
		Min	b.d.	b.d.	b.d.	0.026	b.d.	4.0	0.030	b.d.	b.d.	b.d.	32.8	b.d.	b.d.	b.d.	b.d.	62.6	100.2
3	GS	Mean	b.d.	b.d.	b.d.	0.029	0.193	5.7	b.d.	b.d.	b.d.	b.d.	32.9	b.d.	b.d.	b.d.	b.d.	61.4	100.5
	(350)	SD				0.030	0.321	2.1					0.1					2.2	0.4
		Max	b.d.	b.d.	b.d.	0.061	0.564	7.6	0.044	b.d.	b.d.	b.d.	33.0	b.d.	0.013	b.d.	b.d.	63.5	100.9
		Min	b.d.	b.d.	b.d.	b.d.	b.d.	3.4	b.d.	b.d.	b.d.	b.d.	32.8	b.d.	b.d.	b.d.	b.d.	59.1	100.0
M.d.l.			0.025	0.011	0.007	0.017	0.012	0.0	0.037	0.041	0.015	0.025	0.0	0.009	0.010	0.010	0.011	0.090	

Concentrations from WDS microprobe analyses are expressed in weight %. Results that are below detection are not included in the calculation of mean values. Abbreviations as Table 4. M.d.l.: minimum detection limit. In parentheses, the approximate temperature of equilibration.



Pyrrhotite has an almost identical composition to that in subgreenschist-facies samples (Table 8). Average values of minor elements in chalcopyrite are below detection, but Ag, Hg and Sb were detected in individual grains (Table 5). Sphalerite contains average concentrations of Co and Cu above the limits of detection, and Hg concentrations above detection in individual grains (Table 6). Only one grain of galena was analyzed in greenschist-facies rocks, and minor elements include Ag and Hg (Table 7). Cobaltite, the main host of As and Co, contains detectable Ni and Sb, but Mo and Au were not detected (Table 9).

#### *Amphibolite-facies samples*

Amphibolite-facies samples are coarser grained than the samples at lower metamorphic grades, and the protolith composition is less easily identified. The samples contain quartz, plagioclase, muscovite, biotite,

garnet, titanite, K-feldspar, ilmenite and graphite (Table 1). In the Alpine Schists of New Zealand, the amphibolite facies is defined by the occurrence of biotite, almandine-rich garnet, and oligoclase without albite (Grapes & Watanabe 1992). K-feldspar occurs in the amphibolite-facies rocks of the garnet–oligoclase zone with SiO<sub>2</sub> composition exceeding 70% (Grapes & Watanabe 1992). The absence of rocks with true pelitic compositions has prevented the formation of diagnostic aluminosilicate assemblages, although kyanite–talc and kyanite–zoisite assemblages occur in calc-silicate bands within the garnet–oligoclase zone (Cooper 1980).

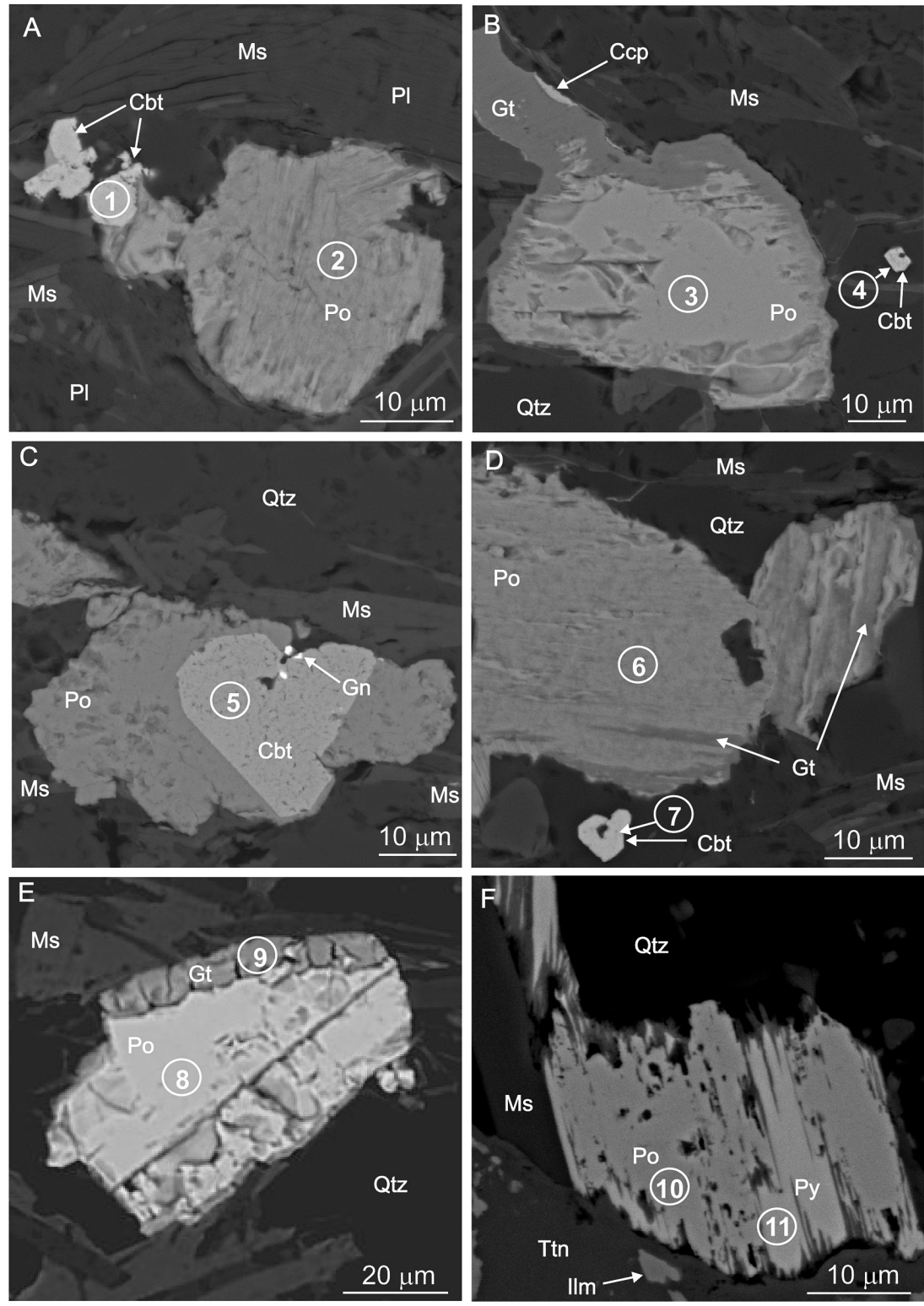
Amphibolite-facies rocks contain abundant pyrrhotite (Figs. 8E, 8F), chalcopyrite, and some fine-grained galena, but pyrite, sphalerite, and cobaltite do not occur (Figs. 2D to 2I, Table 1). Pyrrhotite has a composition similar to that at lower metamorphic grades (Table 8). No single analysis of pyrrhotite yielded Ag, As, Au, Hg, or W above the detection limit, although Sb and Zn concentrations were locally as high as 290 and 360 ppm, respectively (Table 8). Chalcopyrite also contains none of the trace elements sought (Table 5). Although galena occurs in amphibolite-facies rocks, the grain size is too small for WDS microprobe analysis. Likewise, traces of molybdenite occur in amphibolite-facies rocks, but grains are too small for WDS analysis. Post-metamorphic oxidation of pyrrhotite to goethite along grain boundaries and preferential crystallographic planes is common, but chalcopyrite remains unaltered (Figs. 8E, 8F).

## DISCUSSION

#### *Evaluation of retrograde alteration*

An important objective of this study is to evaluate whether the sulfide assemblages described are preserved from peak conditions of metamorphism. Recrystallization of silicate minerals during retrograde cooling is not commonly observed in the Otago and Alpine schists (Bishop 1972, Grapes & Watanabe 1992, Mortimer 2000). Retrograde metamorphic recrystallization in the Alpine Schist has been restricted to some samples from the garnet–oligoclase zone, which show chloritization of garnet and biotite, and growth of phengitic mica (Cooper 1980, Grapes & Watanabe 1995). Previous investigators of sulfide mineralogy have suggested that sulfide minerals quickly re-equilibrate during cooling; the retrograde reaction most commonly described is the sulfidation of pyrrhotite to form pyrite (Barton 1970, Itaya 1975, Kawakami *et al.* 2006). This reaction is not common in the Otago and Alpine schists, and no pyrite is observed in amphibolite-facies samples. Furthermore, the majority of the pyrite observed in unmetamorphosed and subgreenschist-facies rocks shows frambooidal textures typical of marine sediments and sedimentary rocks. In some samples, pyrrhotite is altered along grain

FIG. 5. BSE and RL photomicrographs subgreenschist-facies samples from the Torlesse and Caples terrane. Minerals are labeled and sites of electron-microprobe analyses are shown with trace-element concentrations listed at the side. A. Sample A4 showing a pyrite composite grain with inclusions of galena, sphalerite, and cobaltite (BSE), B. Sample A1, a composite grain of pyrite associated with chalcopyrite, sphalerite and cobaltite (RL), C. Sample A1 showing a composite grain of pyrrhotite with inclusions of galena, cobaltite and chalcopyrite and a mantle of sphalerite (BSE). Note the similarity in texture between this composite grain of pyrrhotite and the composite grain of pyrite in unmetamorphosed samples (Fig. 3D). D. Sample A4 showing an irregular porous aggregate of fine-grained galena, sphalerite and pyrrhotite encapsulated in a frame of massive pyrrhotite (BSE). E and F. Sample A63 showing two composite grains of pyrrhotite with associated chalcopyrite, cobaltite, sphalerite and ullmannite. This was the only grain of ullmannite found (BSE). G and H. Sample A3 showing synkinematic sulfide grains. G shows an aggregate of chalcopyrite, pyrrhotite and sphalerite partially elongate parallel to the foliation. Pyrrhotite and chalcopyrite truncate the foliation, suggesting that at least the outer edges of this mineral grain recrystallized synchronously with foliation development (RL). H. Galena and chalcopyrite grain showing crystal faces typical of recrystallized minerals (RL). Results of analyses: 1) 1250 ppm Co, 950 ppm Ni, 880 ppm As, 150 ppm Sb, 2) 2000 ppm As, 1900 ppm Ni, 1500 ppm Co, 200 ppm Sb, 3) 10000 ppm Ni, 2500 ppm As, 2500 ppm Co, 450 ppm Sb, 4) 800 ppm Co, 640 ppm Hg, 5) 45% As, 29% Co, 2% Ni, 3700 ppm Mo, 1000 ppm Sb, 6) 38% Sb, 18% Ni, 1100 ppm Hg, 160 ppm Ag, 7) 20000 ppm Ni, 1000 ppm Co, 8) 4800 ppm Ni, 1100 ppm Co, 9) 42% As, 27% Co, 2.4% Ni, 1150 ppm Sb, 10) 1100 ppm Hg, 11) 1200 ppm Co, 12) trace elements not detected, 13) 630 ppm Co, 14) 940 ppm Se, 800 ppm Ag, 500 ppm Hg, 90 ppm Au. See Figure 3 for mineral symbols.



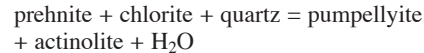
boundaries and preferential crystallographic orientations to goethite (Figs. 6, 8). Alteration to goethite is more common in samples collected from the Southern Alps where rainfall is high, and it is interpreted to have occurred during recent interaction with meteoric water. The limited retrogression observed in the silicate minerals, combined with the dominance of pyrrhotite in middle- to high-grade rocks, imply that the assemblage of sulfide minerals observed has been preserved from peak conditions of metamorphism or close to them.

#### Silicate reactions

Silicate minerals are the major constituent of these rocks and undoubtedly control intensive parameters such as oxygen fugacity. It is likely, therefore, that silicate reactions, particularly those involving Fe-rich minerals, will strongly influence sulfide reactions during prograde metamorphism. Oxygen fugacity is variable on a bed-by-bed basis in the metamorphic pile because of local variations in bulk-rock compositions, but generally decreases with increasing metamorphic grade. The volumetrically minor metacherts are the most oxidized, and these contain oxidized Fe- and Mn-bearing minerals such as hematite, epidote, and piedmontite in the upper greenschist facies. At higher grade, magnetite and spessartine replace these oxidized minerals. Metabasic rocks contain abundant epidote and hematite at the pumpellyite–actinolite facies, develop magnetite in the greenschist facies, and are dominated by hornblende, almandine, and ilmenite at the amphibolite facies. In contrast, varying amounts of

organic matter in the metasedimentary rocks result in variable but low fugacities of oxygen in these rocks, and pyrrhotite occurs locally in low-grade organic-matter-rich argillites (Craw *et al.* 1995).

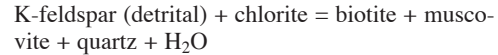
The immature volcanogenic nature of the metasedimentary rocks means that prograde silicate reactions are dominated by Ca, Fe, and Mg minerals, rather than the aluminous minerals commonly found in metamorphosed pelite sequences. The earliest stages of metamorphism involved reactions such as (Bishop 1972):



This reaction was followed by:



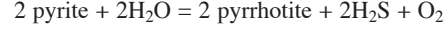
Stilpnomelane was also a common product of a variant of the latter reaction. Biotite appeared in the Southern Alps *via* the reaction:



A similar reaction involving phengitic muscovite or stilpnomelane as a K-bearing reactant occurred in the Otago Schist, where detrital K-feldspar does not persist to the greenschist facies (Brown 1967, Bishop 1972, Grapes 1995, Mortimer 2000). During metamorphism, epidote, actinolite, chlorite, and biotite all become progressively depleted in Fe with increasing grade, and stilpnomelane breaks down in the greenschist facies (Bishop 1972, Grapes & Otsuki 1983). The Fe liberated then contributes to the formation of new  $\text{Fe}^{2+}$ -rich minerals such as almandine (greenschist facies) and ilmenite (amphibolite facies) as metamorphic grade increases.

#### The pyrite–pyrrhotite reaction

Pyrite is common in low-grade metamorphic rocks, and pyrrhotite normally dominates in high-grade rocks, with the transition typically occurring in the greenschist facies (Carpenter 1974, Hall 1986). Sulfide horizons associated with metabasic rocks in the Otago Schist support these observations (Jamieson & Craw 1987). However, our observations (above) show that pyrrhotite appeared at the expense of pyrite in Otago Schist metasedimentary rocks in subgreenschist-facies rocks. The pyrite–pyrrhotite reaction can be expressed as:



This desulfidation reaction is affected by the redox state of the enclosing rock. The Otago Schist metasedimen-

FIG. 6. BSE photomicrographs of subgreenschist-facies samples from Torlesse and Caples terrane. Minerals are labeled and sites of electron-microprobe analyses are shown with trace-element concentrations listed at the side. A, B, C, D, and E. Samples A63, A64, A67, and B84 showing pyrrhotite with cobaltite occurring as either inclusions (A and C), and as euhedral grains proximal pyrrhotite margins (B and D). The pyrrhotite is preferentially altered to goethite along crystallographic planes and rims. The boundaries of the pyrrhotite grains pseudomorphously replaced by goethite truncate the metamorphic foliation and are interpreted to have partially recrystallized during foliation development. F. Torlesse Terrane sample from Oturehua showing pyrite and pyrrhotite coexisting in the same grain. Pyrrhotite is the dominant phase and appears to replace the pyrite that occurs in a central swath and between the sulfide and titanite margin. Results of analyses: 1) 43% As, 28% Co, 560 ppm Sb, 2) 1200 ppm Co, 3) 1000 ppm Co, 4) 41 % As, 31% Co, 1300 ppm Sb, 6) 8000 ppm Co, 7) 45% As, 29% Co, 440 ppm Sb, 8) 1100 ppm Co, 9) 33000 ppm As, 1000 ppm Sb, 900 ppm Co, 250 ppm Se, 210 ppm Mo, 10) 3900 ppm Ni, 2000 ppm Co, 11) 2000 ppm Co, 1400 ppm Ni, 810 ppm Sb. See Figure 3 for mineral symbols.

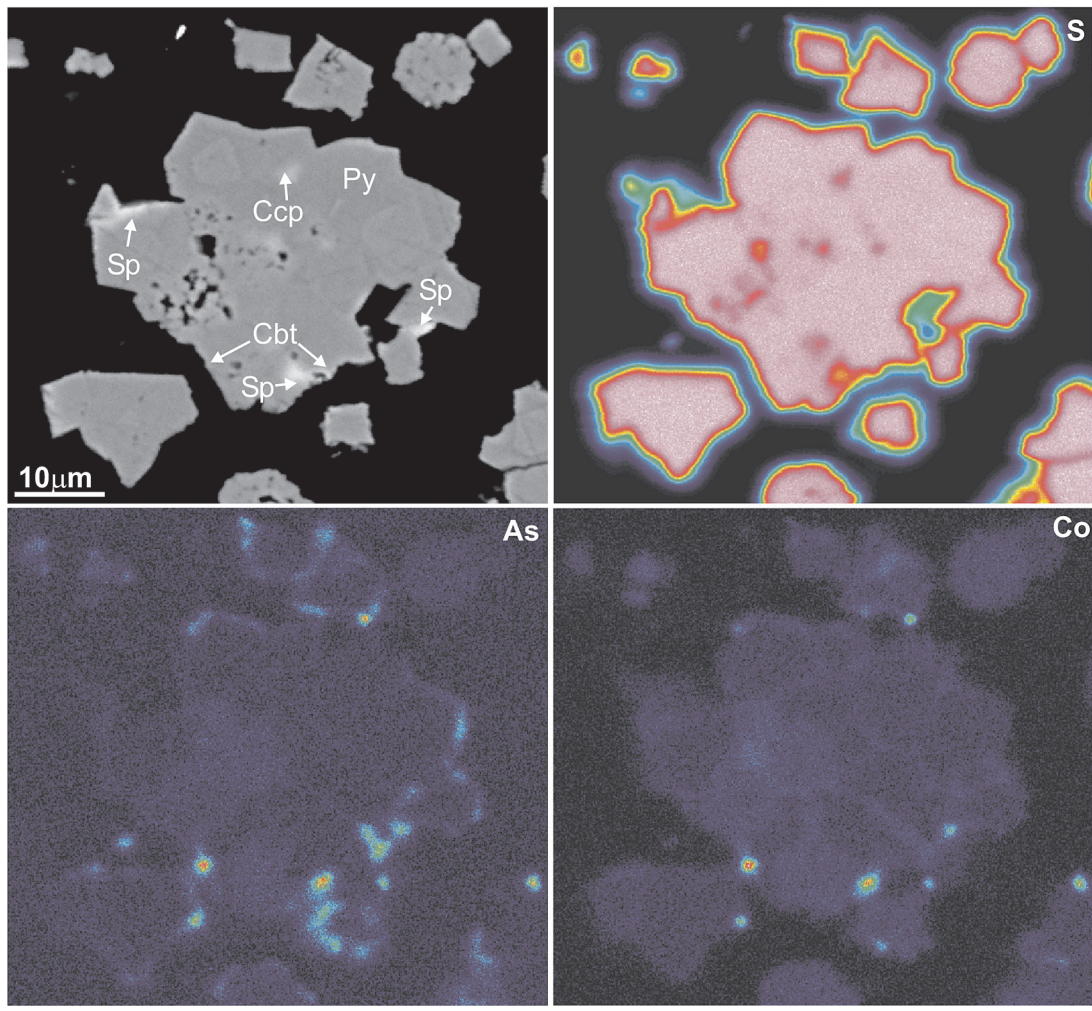


FIG. 7. A BSE image and X-ray elemental maps for S, As, and Co in composite grain of pyrite containing inclusions of sphalerite, chalcopyrite, and cobaltite from sample A4. Brighter colors represent higher concentrations. This grain shows an unusual texture with euhedral recrystallization around subhedral to euhedral and spherical cores. There is a clear association between As and Co; very bright patches represent small inclusions of cobaltite. Arsenic also is enriched in some of the sphalerite patches.

FIG. 8. BSE and RL photomicrographs of sulfide and oxide minerals from greenschist- and amphibolite-facies samples in the Otago and Alpine schists. Minerals are labeled and sites of electron-microprobe analyses are shown with trace-element concentrations listed at the side. A to D are from greenschist-facies samples (A84, B2, B36, C72), and E to H are from amphibolite-facies samples (C61, C76, C56, C59). A. Torlesse terrane sample from Lake Hawea showing synkinematic pyrrhotite with an inclusion of cobaltite (RL). There is no goethite alteration in this sample. B and D. Alpine Schist samples from the Torlesse Terrane, Haast River, showing synkinematic pyrrhotite that has been pervasively, pseudomorphously altered to goethite (RL). C. Torlesse terrane sample from Lake Hawea showing rare synkinematic pyrite. The pyrite occurs either as larger euhedral crystals or smaller irregular crystals that are elongate along the foliation of the rock (RL). E (RL) and F (BSE). Alpine Schist from the Torlesse Terrane, Haast River, showing synkinematic pyrrhotite that has been strongly altered to goethite. Results of analyses: 1) 2600 ppm Ni, 680 ppm Co, 2) 3500 ppm Ni, 710 ppm Co, 3) 41% As, 31% Co, 2% Ni, 390 ppm Sb, 180 ppm Se, 4) 2600 ppm Ni, 2200 ppm Co, 5) 3600 ppm As, 3600 ppm Co, 2800 ppm Ni, 270 ppm Mo, 6) 6700 ppm Sb, 450 ppm As, 380 ppm Se, 180 ppm Co, 110 ppm Au, 7) 3100 ppm Ni, 750 ppm Co, 8) 10000 ppm Co, 6900 ppm Ni, 2900 ppm As, 9) 7600 ppm Ni, 1450 ppm Co, 10) 1300 ppm Ni, 1200 ppm As, 250 ppm Mo, 140 ppm Se, 11) 1900 ppm Ni, 1000 ppm Co, 12) 5000 ppm As, 2000 ppm Ni, 500 ppm Co, 200 ppm Mo. See Figure 3 for mineral symbols.

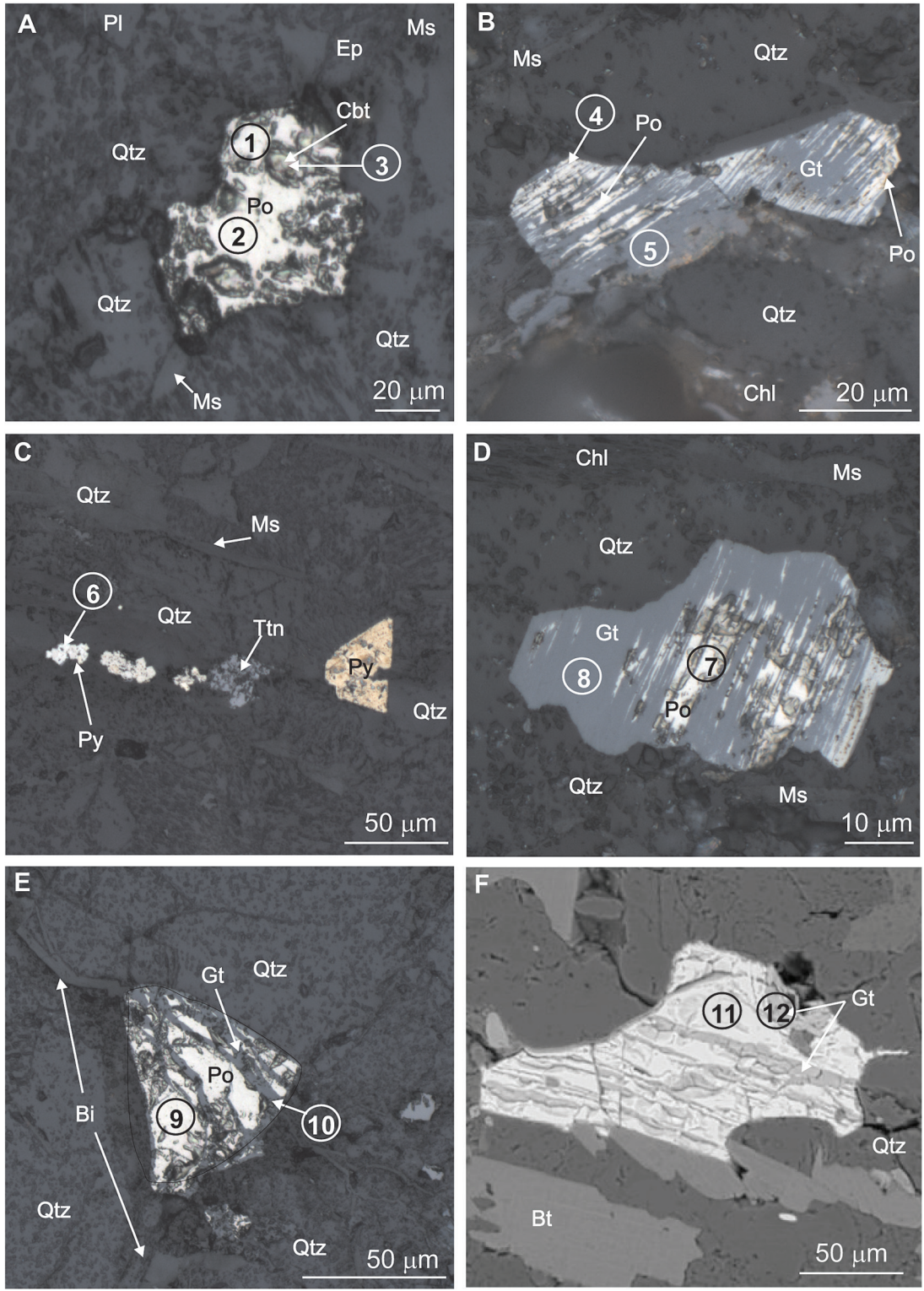


TABLE 7. CHEMICAL COMPOSITION OF GALENA FROM THE OTAGO AND ALPINE SCHISTS, NEW ZEALAND,  
RANKED ACCORDING TO METAMORPHIC GRADE

	N		Ag	As	Au	Co	Cu	Fe	Hg	Mo	Ni	Pb	S	Sb	Se	Si	W	Zn	Total
11	All	Mean	0.059	b.d.	b.d.	b.d.	0.060	0.7	0.078	b.d.	b.d.	84.7	13.2	0.010	0.113	0.366	b.d.	b.d.	99.4
		SD	0.078				0.076	0.6	0.126			1.5	0.2	0.023	0.045	0.572			1.5
		Max	0.233	0.043	0.023	0.057	0.213	1.9	0.451	b.d.	0.161	87.5	13.5	0.077	0.169	1.634	b.d.	b.d.	101.8
		Min	b.d.	81.8	12.6	b.d.	0.025	b.d.	b.d.	b.d.	96.9								
3	Un-met (100)	Mean	b.d.	b.d.	b.d.	b.d.	0.036	0.7	b.d.	b.d.	b.d.	85.1	13.1	b.d.	0.154	0.867	b.d.	b.d.	99.9
		SD					0.027	0.1				2.9	0.4		0.011	0.816			2.7
		Max	b.d.	b.d.	b.d.	b.d.	0.061	0.8	0.059	b.d.	b.d.	87.5	13.4	0.016	0.162	1.634	b.d.	b.d.	101.8
		Min	b.d.	b.d.	b.d.	b.d.	0.5	b.d.	b.d.	b.d.	b.d.	81.8	12.6	b.d.	0.142	b.d.	b.d.	b.d.	96.9
7	Sub (200)	Mean	0.060	b.d.	0.010	b.d.	0.091	0.8	0.110	b.d.	0.030	84.9	13.3	0.015	0.096	0.174	b.d.	b.d.	99.6
		GS	0.059		0.008		0.092	0.8	0.168		0.064	0.7	0.1	0.031	0.049	0.320			0.7
		SD																	
		Max	0.148	0.033	0.023	0.057	0.213	1.9	0.451	b.d.	0.161	86.0	13.5	0.077	0.169	0.808	b.d.	b.d.	100.1
		Min	b.d.	84.2	13.1	b.d.	0.025	b.d.	b.d.	b.d.	98.3								
1	GS (350)	Mean	0.233	0.043	b.d.	b.d.	0.1	0.068	b.d.	b.d.	84.7	13.1	b.d.	0.120	b.d.	b.d.	b.d.	b.d.	98.5
		SD																	
		Max	0.233	0.043	b.d.	b.d.	0.1	0.068	b.d.	b.d.	84.7	13.1	b.d.	0.120	b.d.	b.d.	b.d.	b.d.	98.5
		Min	0.233	0.043	b.d.	b.d.	0.1	0.068	b.d.	b.d.	84.7	13.1	b.d.	0.120	b.d.	b.d.	b.d.	b.d.	98.5
	M.d.l.		0.034	0.016	0.010	0.025	0.022	0.1	0.060	0.057	0.027	0.096	0.0	0.010	0.015	0.015	0.036	0.035	

Concentrations from WDS microprobe analyses are expressed in weight %. Results that are below detection are not included in the calculation of mean values. Abbreviations as Table 4. M.d.l.: minimum detection limit. In parentheses, the approximate temperature of equilibration.

TABLE 8. CHEMICAL COMPOSITION OF PYRRHOTITE FROM THE OTAGO AND ALPINE SCHISTS, NEW ZEALAND,  
RANKED ACCORDING TO METAMORPHIC GRADE

	N		Ag	As	Au	Co	Cu	Fe	Hg	Mo	Ni	Pb	S	Sb	Se	Si	W	Zn	Total
95	All	Mean	b.d.	b.d.	b.d.	0.103	0.027	59.1	b.d.	b.d.	0.369	b.d.	39.1	b.d.	b.d.	0.030	b.d.	b.d.	98.7
		SD				0.043	0.180	1.0			0.237		0.6			0.083			1.0
		Max	b.d.	b.d.	b.d.	0.227	1.763	60.3	0.056	b.d.	1.174	b.d.	41.0	0.048	0.024	0.597	0.033	0.046	100.0
		Min	b.d.	b.d.	b.d.	0.004	b.d.	52.6	b.d.	b.d.	b.d.	b.d.	37.7	b.d.	b.d.	b.d.	b.d.	b.d.	95.9
50	Sub (200)	Mean	b.d.	b.d.	b.d.	0.111	0.047	58.9	b.d.	b.d.	0.397	b.d.	39.4	b.d.	b.d.	0.031	b.d.	b.d.	98.6
		GS	0.049	0.246	1.3						0.254		0.5			0.084			0.9
		SD																	
		Max	b.d.	b.d.	b.d.	0.227	1.763	60.1	0.056	b.d.	1.071	b.d.	41.0	0.048	0.017	0.597	0.033	0.033	100.0
		Min	b.d.	b.d.	b.d.	0.004	b.d.	52.6	b.d.	b.d.	b.d.	b.d.	38.3	b.d.	b.d.	b.d.	b.d.	b.d.	95.9
17	GS (350)	Mean	b.d.	b.d.	b.d.	0.067	b.d.	59.7	b.d.	b.d.	0.340	b.d.	39.4	b.d.	b.d.	b.d.	b.d.	b.d.	99.5
		SD				0.023		0.4			0.091		0.2						0.4
		Max	b.d.	b.d.	b.d.	0.123	b.d.	60.2	b.d.	b.d.	0.578	b.d.	39.7	0.012	0.015	b.d.	b.d.	0.046	100.0
		Min	b.d.	b.d.	b.d.	0.028	b.d.	58.7	b.d.	b.d.	0.190	b.d.	38.9	b.d.	b.d.	b.d.	b.d.	b.d.	98.1
28	Amph (575)	Mean	b.d.	b.d.	b.d.	0.110	b.d.	59.3	b.d.	b.d.	0.370	b.d.	38.5	b.d.	b.d.	b.d.	b.d.	b.d.	98.4
		SD				0.026		0.5			0.285		0.5						1.0
		Max	b.d.	b.d.	b.d.	0.167	0.034	60.3	b.d.	b.d.	1.174	b.d.	39.4	0.029	0.024	b.d.	b.d.	0.036	99.9
		Min	b.d.	b.d.	b.d.	0.062	b.d.	57.8	b.d.	b.d.	0.067	b.d.	37.7	b.d.	b.d.	b.d.	b.d.	b.d.	95.9
	M.d.l.		0.024	0.012	0.008	0.019	0.015	0.0	0.036	0.056	0.016	0.032	0.0	0.008	0.012	0.010	0.023	0.022	

Concentrations from WDS electron-microprobe analyses are in weight %. Results that are below detection are not included in the calculation of mean values. Abbreviations as Table 4. M.d.l.: minimum detection limit. In parentheses, the approximate temperature of equilibration.

tary rocks are relatively reduced compared to metabasic rocks, particularly where organic material is abundant (see previous section). Hence, the low-grade appearance of pyrrhotite in the Otago metasedimentary rocks prob-

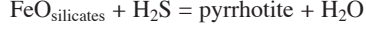
ably arises because of organic-matter-driven reducing conditions during metamorphism, as has been observed elsewhere (Frost 1979, Ferry 1981, Mohr & Newton 1983, Hall *et al.* 1987).

TABLE 9. CHEMICAL COMPOSITION OF COBALTITE FROM THE OTAGO AND ALPINE SCHISTS, NEW ZEALAND,  
RANKED ACCORDING TO METAMORPHIC GRADE

N		Ag	As	Au	Co	Cu	Fe	Hg	Mo	Ni	Pb	S	Sb	Se	Si	W	Zn	Total		
20	All	Mean	b.d.	39.7	b.d.	27.8	0.101	5.3	b.d.	2.200	0.072	21.0	0.058	b.d.	1.009	b.d.	b.d.	97.2		
		SD		5.1		3.8	0.283	3.1		0.585	0.238	0.9	0.038		1.548			3.1		
		Max	b.d.	44.6	0.011	32.7	1.309	16.0	0.067	0.369	2.935	0.790	23.4	0.128	0.058	5.637	b.d.	0.042	100.8	
		Min	b.d.	24.2		b.d.	18.1	b.d.	2.8	b.d.	b.d.	1.356	b.d.	18.7	b.d.	b.d.	0.035	b.d.	b.d.	90.2
11	Sub	Mean	b.d.	38.3	b.d.	26.1	0.139	5.5	b.d.	b.d.	2.127	0.113	20.8	0.078	b.d.	1.391	b.d.	b.d.	95.6	
	GS	SD		6.4		3.9	0.371	4.1			0.596	0.299	1.2	0.037		1.750			3.0	
	(200)	Max	b.d.	44.6	0.011	31.2	1.309	16.0	0.067	0.369	2.805	0.790	23.4	0.128	0.058	5.637	b.d.	0.042	100.8	
		Min	b.d.	24.2		b.d.	18.1	b.d.	2.8	b.d.	b.d.	1.356	b.d.	18.7	b.d.	b.d.	0.103	b.d.	b.d.	90.2
9	GS	Mean	b.d.	41.7	b.d.	30.0	0.050	5.0	b.d.	b.d.	2.327	b.d.	21.3	0.031	b.d.	0.169	b.d.	b.d.	99.4	
	(350)	SD		1.1		2.4	0.078	0.8			0.630		0.4	0.019		0.207			1.1	
		Max	b.d.	43.4	b.d.	32.7	0.238	6.0	b.d.	b.d.	2.935	b.d.	21.9	0.069	0.039	0.536	b.d.	b.d.	100.6	
		Min	b.d.	39.9	b.d.	26.2	b.d.	4.0	b.d.	b.d.	1.588	b.d.	20.6	0.008	b.d.	0.035	b.d.	b.d.	97.8	
	M.d.l.			0.027	0.027	0.007	0.023	0.017	0.0	0.040	0.080	0.019	0.022	0.0	0.008	0.017	0.010	0.017	0.024	

Concentrations from WDS electron-microprobe analyses are expressed in weight %. Results that are below detection are not included in the calculation of mean values. Abbreviations as Table 4. M.d.l.: minimum detection limit. In parentheses, the approximate temperature of equilibration.

The H<sub>2</sub>S released by the pyrite–pyrrhotite reaction may remain in the fluid, thereby increasing the sulfur fugacity (Ferry 1981). Alternatively, the H<sub>2</sub>S may react with the enclosing silicates, resulting in localized sulfidation of the rock. Prograde silicate reactions release Fe (above), that could combine with the H<sub>2</sub>S to form more pyrrhotite:



Atomic Fe and S concentrations and Fe/S values for pyrite and pyrrhotite are plotted in Figure 9. Changes in Fe/S in pyrite are controlled by changes in the Fe content, which decreases between unmetamorphosed and subgreenschist-facies samples, and increases in greenschist-facies samples (Fig. 9). In pyrrhotite, however, Fe/S increases with increasing metamorphic grade primarily because of decreasing S content. The mobilization of Fe by metamorphic reactions may therefore be more important at lower metamorphic grades, whereas at higher metamorphic grades, the removal of S appears to be a more important process. The decrease in the S content of pyrrhotite may be caused either by removal of S by fluids produced by metamorphic dehydration, or a slight modal increase in the amount of pyrrhotite, as is suggested by Figure 2. The whole-rock concentrations of S show no systematic change in average concentrations with increasing metamorphic grade, suggesting that most of the H<sub>2</sub>S released by the pyrite–pyrrhotite reaction, and by the progressive decrease of S content in pyrrhotite, was locally remobilized and retained in the rock (Fig. 2). The decrease in the S content of pyrrhotite may be an indication of

progressive decrease of oxygen fugacity with increasing metamorphic grade.

#### Sulfide minerals as hosts for trace metals

By comparing concentrations of sulfur, metals and semi-metals in sulfide minerals with those in the whole rock, it is possible to evaluate the relative importance of the sulfides as host minerals for these elements. The accuracy of this mass balance is compromised by 1) the large range in concentrations of certain minor and trace elements in the sulfides, and 2) any compositional disparity between a two-dimensional thin section and an aliquot of sample powder used for whole-rock analyses. For example, As concentrations in pyrite range from below the detection limit (120 ppm) up to over 13000 ppm (Table 4), and Figures 4 and 7 attest to the heterogeneous distribution of As within individual grains. There will always be a degree of compositional disparity between the mineralogy and mineral composition represented on a thin section and a whole-rock analysis. However, the reasonable correlation between total sulfide calculated from SEM scans and whole-rock S concentration suggests that the two are generally proportional (Fig. 2a), allowing for a mass-balance calculation (Table 10).

The mass balance was calculated using the whole-rock concentrations and sulfide abundances for each sample as listed in Table 2, and the mean elemental concentrations in each type of sulfide mineral at the relevant metamorphic grade (Tables 4 to 9). The mass balance has been calculated only for elements whose mean concentration is above the limit of detection in one

or more of the sulfide minerals. The mass balance shows that the proportion of metals hosted in sulfide minerals is highly variable and commonly considerably less than 100% (Table 10, Fig. 10). The proportion of Fe in sulfide minerals is low, ranging from 0.1 to 3%, whereas the proportion of S in sulfide minerals is high, ranging from 2 to 156% (Table 10). This is not surprising, as many minerals host Fe in these rocks, such as chlorite, biotite, amphiboles and Fe oxides, whereas there are few minerals other than the sulfides that host S. Barite occurs in unmetamorphosed and subgreenschist-facies samples (Table 1, Fig. 2), but has not been observed in the samples at a higher metamorphic grade. Correspondingly, the proportion of S in sulfide minerals increases with increasing metamorphic grade, most likely owing to the progressive reduction of  $\text{SO}_4$  from barite. Copper

shows a similar trend to S, with the proportion of Cu in sulfide minerals ranging from 0.1 to 151% (Table 10). The average proportion of Cu hosted in sulfide minerals increases with metamorphic grade (Fig. 10), suggesting that chalcopyrite becomes a very important host of Cu in metamorphic rocks. This finding is consistent with the petrographic observations that chalcopyrite is persistent through high-grade metamorphic conditions (Tables 1, 2, and 5).

The proportions of Zn, Pb, Co and As in sulfide minerals are also highly variable and are strongly influenced by the decrease in abundance of sphalerite,

TABLE 10. MASS BALANCE BETWEEN THE TOTAL ELEMENTAL ABUNDANCE IN SULFIDE MINERALS AND MEASURED WHOLE-ROCK CONCENTRATION

Sample	Meta-morphic grade	Temp. °C	Total elemental abundance in sulfide minerals relative to whole-rock concentration (%)						
			S	Fe	Cu	Zn	Pb	Co	As
C46	Un-met	100	104	0.6	71	0.1	1	5	36
C48	Un-met	100	15	0.1	15	30	2	0.5	8
C47	Un-met	100	5	0.1	5	0.3	2	0.5	3
C5	Un-met	100	2	0.1	13	0.1	0.7	0.1	1
A6	Un-met	100	65	1	39	4	89	22	85
Mean			38.2	0.4	28.6	6.9	18.9	6.9	26.6
SD			44.7	0.4	26.9	13.0	39.2	10.3	35.6
A1	Sub-GS	200	83	0.4	28	22	17	38	
A3	Sub-GS	200	8	0.1	11	13	0.1	5	3
A4	Sub-GS	200	32	0.2	15	22	75	36	135
A5	Sub-GS	200	111	1	35	8	36	33	
A60	Sub-GS	200	118	0.4	26	11	15	41	50
A63	Sub-GS	200	27	0.2	12	1	0.1	2	1
A64	Sub-GS	200	40	0.2	20	9	3	17	22
A67	Sub-GS	200	32	0.3	7	6	21	10	
B84	Sub-GS	200	70	3	136	2	4	34	50
Mean			57.9	0.6	36.7	14.2	14.8	23.2	38.0
SD			39.2	0.9	49.0	11.7	23.7	14.2	40.9
A84	GS	350	34	0.3	59	2	3	6	
B2	GS	350	73	3	18	33	0.1	35	112
B18	GS	350	36	1	0.1	0.1	54	1	
B36	GS	350	67	0.3	37	1	4	6	
C69	GS	350	45	0.4	162	1	9	5	
C72	GS	350	54	0.2	69	0.1	1	0.1	
Mean			51.5	0.9	57.5	6.2	11.9	18.0	21.7
SD			16.1	1.1	57.1	13.1	20.9	24.0	44.3
C61	Amph	575	90	0.5	8	0.1	6	3	0
C76	Amph	575	30	1	126	0.1	0	0	
C56	Amph	575	25	1	117	0.1	1	5	0
C59	Amph	575	156	3	151	0.1	2	21	0
Mean			75.3	1.4	100.5	0.1	2.3	9.7	0.0
SD			61.4	1.1	63.3	0.0	2.6	9.9	0.0

For each sample, the element concentration in each type of sulfide mineral (Tables 4 to 9) is multiplied by its abundance (Table 2), and the sum for all sulfide mineral types is divided by the whole-rock concentration (Table 2). The result is a percentage value for the total elemental abundance from sulfide minerals compared to the whole-rock concentration in each sample.

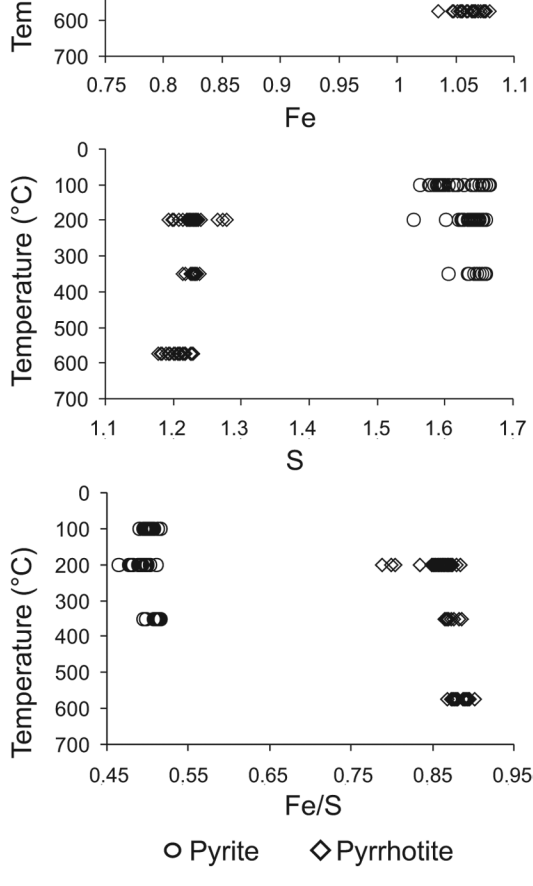


FIG. 9. Atomic Fe, S and Fe/S values in pyrite (circles) and pyrrhotite (diamonds) versus metamorphic temperature.

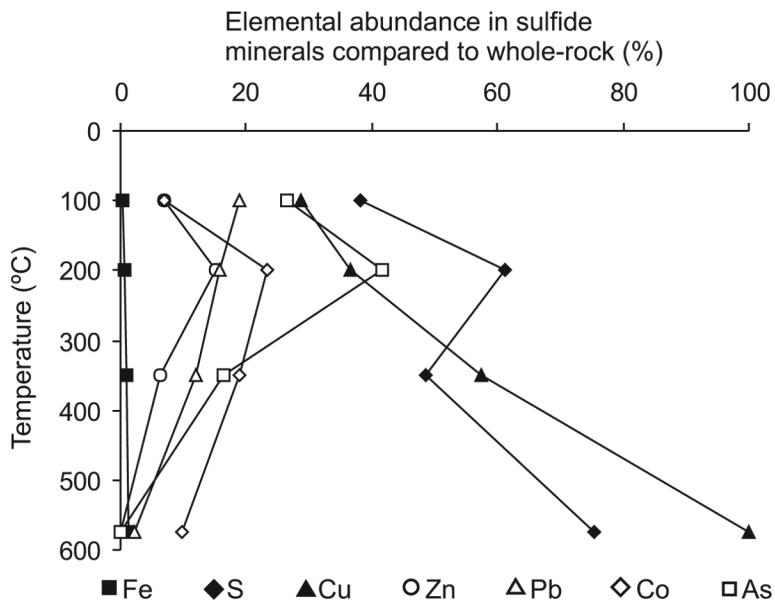


FIG. 10. The abundances of S, Fe, Cu, Zn, Pb, Co, and As in sulfide minerals compared to whole-rock values (%) versus metamorphic temperature. Mean values from Table 10 are plotted. See Table 10 for the range in values and the standard deviations.

galena, and cobaltite with increasing metamorphic grade (Fig. 10). Sphalerite and galena are the major sulfide hosts of Zn and Pb, respectively, but these minerals host a relatively minor proportion of these elements in the whole rock, particularly at middle to high metamorphic grades (Table 10, Fig. 10). The proportion of As and Co in sulfide minerals in individual samples ranges from below detection up to 135%, and the average proportion of these elements within sulfides decreases with increasing metamorphic grade (Table 10, Fig. 10). Pyrite and cobaltite are important host minerals for As and Co, but these minerals do not occur at high metamorphic grades.

There are too few analyses of samples for gold above the detection limit for a meaningful mass-balance. However, it is clear that 90 and 100 ppm Au must be orders of magnitude higher than the average concentration in sulfide minerals. For example, sample A4 has one determination of Au in sulfide at 100 ppm, its whole-rock Au concentration is 7 ppb, and pyrite makes up 0.01% of the sample. If all the pyrite in this sample had a concentration of 100 ppm, the whole-rock concentration would be 1 ppm, almost ore grade. If we assume that all of the Au is hosted in pyrite, then the average Au concentration in the pyrite would have to be less than 1 ppm to give the correct whole-rock concentrations.

In summary, as metamorphism progresses and detrital minerals are recrystallized into authigenic

mineral phases, sulfide minerals become increasingly important minerals hosts for S, Cu, Zn, Pb, As, and Co in low- to middle-grade rocks (Table 10, Fig. 10). Pyrrhotite and chalcopyrite become the main host minerals for S and Cu in middle- to high-grade rocks (Table 10, Fig. 10). However, sphalerite, galena, and cobaltite become less important host phases for Zn, Pb, As and Co, as these minerals become less abundant in middle- to high-grade rocks (Table 10, Fig. 10).

#### *Metal enrichment in sulfides at low metamorphic grades*

The variations in abundances of Au, Ag, As, Sb, and Hg in sulfide minerals from unmetamorphosed to amphibolite-facies metamorphic conditions are summarized in Figure 11 and reported in Tables 4, 5, 6, 7, 8, and 9. Arsenic and Sb in spherical and composite pyrite, Ag, Au, Hg, Sb, and Se in galena, and Hg in sphalerite all increase in concentration in subgreenschist facies compared to unmetamorphosed rocks. Silver and As concentrations in galena also increase between subgreenschist- and greenschist-facies rocks (Table 6, Fig. 11).

The increases in trace-element concentrations in sulfides during low-grade metamorphism can be explained either through enrichment from an external metal-rich fluid, or localized redistribution and concentration of elements from more abundant phases that

contain lower concentrations of the trace elements. If the metals were introduced by external fluids, one would expect to see an increase in average whole-rock concentrations of the enriched elements, whereas localized remobilization of metals would cause a larger range of values, but no increase in average whole-rock concentration in subgreenschist-facies samples. Silver, As, and Sb show a greater range of concentrations in whole-rock samples from subgreenschist and green-

schist facies than in unmetamorphosed rocks, but no significant change on average (Fig. 12; Pitcairn *et al.* 2006a). Gold and Hg show a decrease in concentrations between subgreenschist and greenschist facies (Fig. 12). Whole-rock analyses of samples for Ag are very close to the detection limit, 0.03 ppm; therefore, we cannot determine the true range of whole-rock concentrations for this element (Fig. 12; Pitcairn *et al.* 2006a). Local-scale redistribution of trace elements during recrystall-

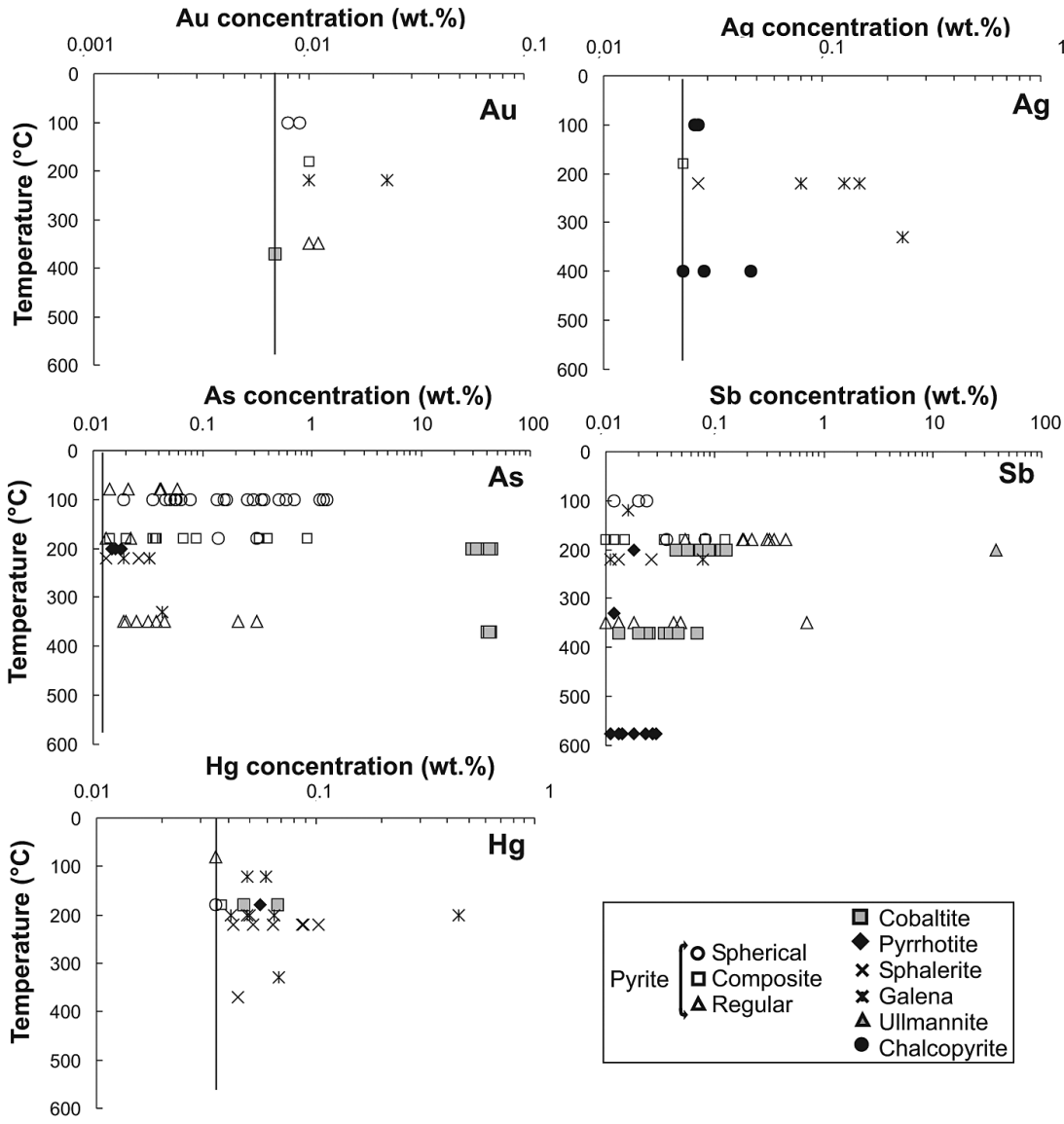


FIG. 11. Concentrations of Au, As, Sb, Ag, and Hg in sulfide minerals plotted against metamorphic temperature of host rocks. The black lines on each plot indicate the lowest limit of detection for each element; limits of detection vary among minerals (see Table 2).

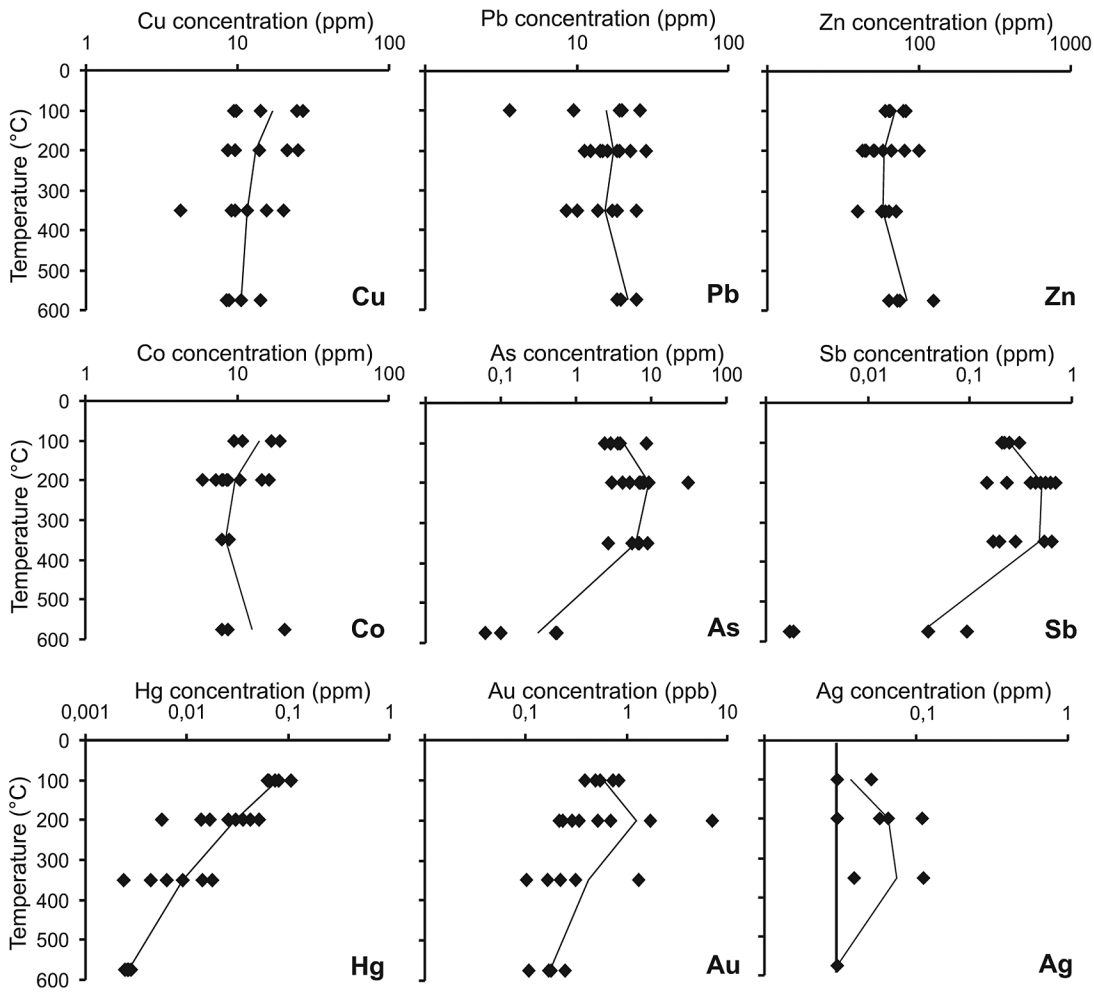


FIG. 12. Whole-rock concentrations of Cu, Pb, Zn, Co, As, Sb, Hg, Au, and Ag *versus* metamorphic temperature for all samples used in this study. Black lines represent mean values at each metamorphic grade. The thicker black line in the Ag diagram shows the detection limit for that element.

lization in subgreenschist-facies rocks thus seems the cause of trace-element enrichments in sulfide minerals in these rocks. Chemical changes between unmetamorphosed rocks and subgreenschist and greenschist facies are accompanied by a clear textural change, best displayed by Fe sulfide minerals, from spherical to composite and synkinematic textures, an increase in the amount of pyrrhotite, and a decrease in the amount of pyrite (Fig. 2). Pyrrhotite has much lower concentrations of trace elements compared to pyrite. Replacement of some grains of the relatively trace-element-rich pyrite by pyrrhotite may have led locally to the incorporation of the liberated trace elements in the other sulfides formed during this replacement. The tectonic fabrics generated during metamorphism and deformation may

play an important role in localized mobility of elements during low-grade metamorphism.

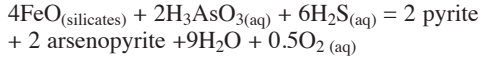
#### *Metal mobility at middle to high metamorphic grades*

Whole-rock analyses show that there has been a decrease in bulk Ag, As, Au, Hg, and Sb concentrations with increasing metamorphic grade in the Otago and Alpine schists (Fig. 12; Pitcairn *et al.* 2006a). These decreases in bulk concentrations broadly correlate with the decreasing abundance of pyrite, cobaltite, sphalerite and galena between subgreenschist and amphibolite facies (Fig. 2). We suggest that the decreases in whole-rock metal content are caused, at least in part, by the decreasing stability of the sulfide host minerals

pyrite, cobaltite, sphalerite and galena at greenschist- to amphibolite-facies metamorphic grades. Arsenic displays an abrupt decrease in bulk As content from ~10 ppm at greenschist facies and below, to <1 ppm As in amphibolite facies (Fig. 12; Campbell *et al.* 2004, Pitcairn *et al.* 2006a). The decrease in the abundance of pyrite and cobaltite, which are important host minerals for As, is more gradual, and begins at lower metamorphic grade than the large depletion in whole-rock As concentrations at between the greenschist and amphibolite facies. Minerals other than the sulfides thus may host As in greenschist-facies rocks. It is possible that hydrous silicates such as chlorite and muscovite host As in greenschist-facies rocks, and that the abrupt decrease in As concentrations is caused by release of As to aqueous fluid during dehydration reactions. There has been no corresponding depletion in bulk Co content of the amphibolite-facies whole-rocks (Fig. 12), suggesting that Co has been incorporated into other minerals in the greenschist- and amphibolite-facies rocks such as pyrrhotite and silicate minerals.

Large volumes of metamorphic fluids were produced at the greenschist–amphibolite transition in the Otago and Alpine schists (Pitcairn 2004, Pitcairn *et al.* 2006a), owing mainly to the breakdown of chlorite and organic matter (Pitcairn *et al.* 2005a, 2005b). Elevated temperatures combined with the presence of large volumes of aqueous fluids may have caused the instability of cobaltite and sphalerite, and the leaching of mobile elements from other minerals, such as galena.

The widespread occurrence of gold deposits, enriched in As, W, Sb, and S, through the Otago and Alpine schists (Fig. 1), attests to at least some mobility of elements during metamorphism (Craw 2002, Pitcairn *et al.* 2006a). In particular, the Macraes gold deposit (Fig. 1) is a late metamorphic deposit formed *via* structurally mediated retrograde metamorphic reactions (Craw 2002). Mineralization resulted from sulfidation reactions between fluid and the silicates in the host schist, such as:



This reaction (modified after Craw 2002) is similar to the prograde sulfidation of silicates to form additional pyrrhotite that is proposed above.

## CONCLUSIONS

Sulfide minerals in the Otago and Alpine schists underwent systematic changes in abundance, composition and texture during prograde metamorphism. The key changes are summarized below and illustrated in Figure 13.

1) There was a textural change from spherical pyrite in unmetamorphosed rocks to irregular composite sulfides in subgreenschist-facies rocks. This partially

controls remobilization of trace elements into cobaltite, sphalerite and galena.

2) The trace-element concentrations in cobaltite, sphalerite and galena increased between unmetamorphosed rocks and the subgreenschist facies. Although locally remobilized, these elements are not removed from the rock at these metamorphic grades.

3) There was a replacement of pyrite by pyrrhotite in subgreenschist- and greenschist-facies rocks. Pyrite hosts a wide variety of trace elements, commonly at significant concentrations. In contrast, trace-element substitution into pyrrhotite is much more restricted. Consequently, the phase change from pyrite to pyrrhotite resulted in the remobilization of trace elements into other sulfide phases such as cobaltite, sphalerite and galena.

4) Pyrite, sphalerite, and cobaltite disappeared between the greenschist and amphibolite facies. These minerals host abundant trace elements, and their absence at higher metamorphic grades has exerted a strong control on the mobility of Ag, Au, As, Hg, and Sb. However, a mass balance between sulfide minerals and whole rocks shows that minerals other than sulfides must host a proportion of the As.

5) The stability of different sulfide minerals during prograde metamorphism is important for the formation of orogenic gold deposits. The recrystallization of sulfide minerals retained the ore-forming trace elements in the rocks until the major period of generation of metamorphic fluid, when these elements were then liberated from the host minerals and transported in the fluids to the site of deposition to form the orogenic gold deposits in the Otago and Alpine schists.

## ACKNOWLEDGEMENTS

We thank Lang Shi for assistance with electron-microprobe analyses at McGill University, Montreal. Samples were collected as part of Ph.D. research for which IKP acknowledges receipt of NERC studentship NER/S/A/2000/03626. Whole-rock analyses performed at the NOC were supported by the Nuffield Foundation Grant NAL/00392/G and other funds to DAHT. The Challenger Division for Seafloor Processes (NOC) assisted with the analyses of samples for Hg, As, Sb, and Se. IKP also acknowledges Vetenskapsrådet personal research grant (1420701). GRO acknowledges an NSERC Discovery grant, and a Premier Research Excellence Award (PREA) that supported this research. Stockholm University acknowledges funding from Wallenberg Foundation for upgrading the Philips ESEM. The University of Otago provided partial support for fieldwork. We also thank the referees Richard J. Goldfarb and Richard I. Grauch and Associate Editor David Mossman for providing insightful comments that greatly improved the quality of the manuscript.

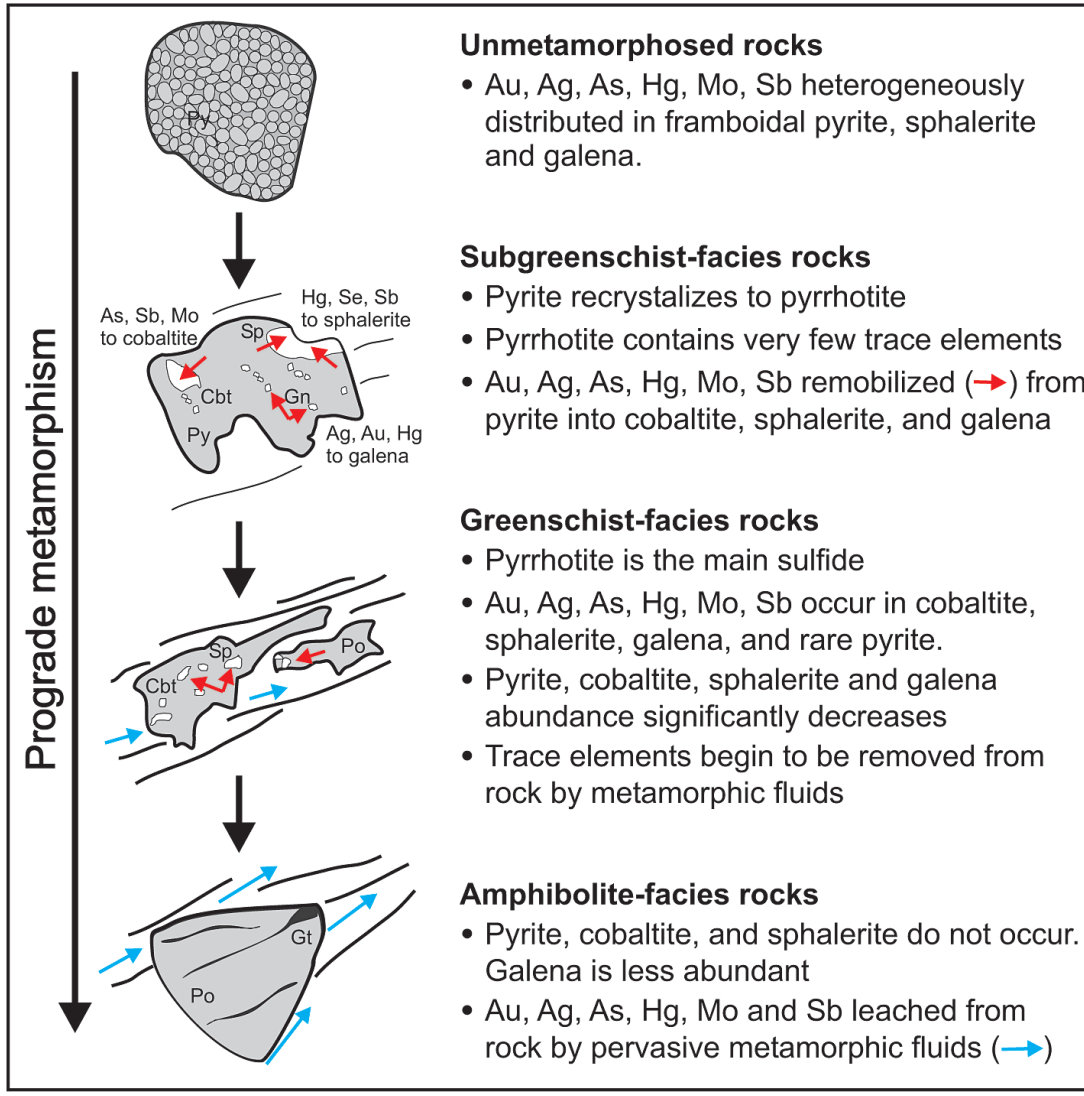


FIG. 13. Schematic diagram showing the proposed model for trace-element mobility during evolution of sulfide minerals during prograde metamorphism of the Otago and Alpine schists. Red arrows represent element mobility, and blue arrows represent flow of metamorphic fluid. Mineral symbols as in Figure 3.

#### REFERENCES

- ADAMS, C.J. & GRAHAM, I.J. (1997): Age of metamorphism of the Otago Schist in eastern Otago and determination of protoliths from initial strontium isotope characteristics. *N.Z. J. Geol. Geophys.* **40**, 275-286.
- ALMEIDA, C.M., OLIVO, G.R., CHOUINARD, A., WEAKLY, C. & POIRIER, G. (2010): Mineral paragenesis, alteration and metal zoning of the two types of gold ore from the Carlin-type deposits in the southern part of the Goldstrike property, northern Nevada: implications for source of ore-forming elements, ore genesis and mineral exploration. *Econ. Geol.* **105**, 971-1004.
- BARTON, P.B., JR. (1970): Sulfide petrology. *Mineral. Soc. Am., Spec. Pap.* **3**, 187-198.
- BERNER, R.A. (1970): Sedimentary pyrite formation. *Am. J. Sci.* **268**, 1-23.

- BISHOP, D.G. (1972): Progressive metamorphism from prehnite–pumpellyite to greenschist facies in the Dansey Pass area, Otago, New Zealand. *Geol. Soc. Am., Bull.* **83**, 3177–3198.
- BISHOP, D.G., BRADSHAW, J.D. & LANDIS, C.A. (1985): Provisional terrane map of the South Island, New Zealand. In *Tectonostratigraphic Terranes of the Circum-Pacific Region* (D.G. Howell, ed.). AAPG *Circum-Pacific Council for Energy and Mineral Resources, Earth Science Series* **1**, 515–521.
- BROWN, E.H. (1967): The greenschist facies in part of eastern Otago, New Zealand. *Contrib. Mineral. Petrol.* **14**, 259–292.
- BROWN, J.L., ELLIS, D.J., ARCUS, R.J. & CHRISTY, A.G. (2006): Prograde sulfide metamorphism and sulfide–silicate phase relations in blueschist and eclogite, New Caledonia. *Geochim. Cosmochim. Acta* **70**, Supp. 1, A69.
- CAMPBELL, J.R., CRAW, D., FREW, R., HORTON, T. & CHAMBERLAIN, C.P. (2004): Geochemical signature of orogenic hydrothermal activity in an active tectonic intersection zone, Alpine Fault, New Zealand. *Mineral. Deposita* **39**, 437–451.
- CARPENTER, R.H. (1974): Pyrrhotite isograd in southeastern Tennessee and southwestern North Carolina. *Geol. Soc. Am., Bull.* **85**, 451–456.
- COOMBS, D.S., LANDIS, C.A., NORRIS, R.J., SINTON, J.M., BURNS, D.J. & CRAW, D. (1976): The Dun Mountain Ophiolite Belt, New Zealand, its tectonic setting, constitution and origin, with special reference to the southern portion. *Am. J. Sci.* **276**, 561–603.
- COOPER, A.F. (1980): Retrograde alteration of chromium kyanite in metachert and amphibolite whiteschist from the Southern Alps, New Zealand, with implications for uplift on the Alpine fault. *Contrib. Mineral. Petrol.* **75**, 153–164.
- CRAIG, J.R. & VOKES, F.M. (1993): The metamorphism of pyrite and pyritic ores: an overview. *Mineral. Mag.* **57**, 3–18.
- CRAW, D. (2002): Geochemistry of late metamorphic hydrothermal alteration and graphitisation of host rock, Macraes gold mine, Otago Schist, New Zealand. *Chem. Geol.* **191**, 257–275.
- CRAW, D., HALL, A.J., FALICK, A.E. & BOYCE, A.J. (1995): Sulphur isotopes in a metamorphogenic gold deposit, Macraes mine, Otago Schist, New Zealand. *N.Z. J. Geol. Geophys.* **38**, 131–136.
- CRAW, D., WINDLE, S.J. & ANGUS, P.V. (1999): Gold mineralization without quartz veins in a ductile–brittle shear zone, Macraes Mine, Otago Schist, New Zealand. *Mineral. Deposita* **34**, 382–394.
- DILL, H. & KEMPER, E. (1990): Crystallographic and chemical variations during pyritization in the upper Barremian and lower Aptian claystones from the lower Soxoian Basin (NW Germany). *Sedimentology* **37**, 427–443.
- FERRY, J.M. (1981): Petrology of graphitic sulfide-rich schists from south-central Maine: an example of desulfidation during prograde regional metamorphism. *Am. Mineral.* **66**, 908–930.
- FROST, B.R. (1979): Mineral equilibria involving mixed-volatiles in a C–O–H fluid phase; the stabilities of graphite and siderite. *Am. J. Sci.* **279**, 1033–1059.
- GRAHAM, U.M. & ROBERTSON, J.D. (1995): Micro-PIXE analysis of frambooidal pyrite and associated maceral types in oil shale. *Fuel* **74**, 530–535.
- GRAPES, R.H. (1995): Uplift and exhumation of Alpine Schist, Southern Alps, New Zealand: thermobarometric constraints. *N.Z. J. Geol. Geophys.* **38**, 525–533.
- GRAPES, R.H. & OTSUKI, M. (1983): Peristerite compositions in quartzofeldspathic schists, Franz Josef – Fox Glacier area, New Zealand. *J. Metam. Geol.* **1**, 47–61.
- GRAPES, R. & WATANABE, T. (1992): Metamorphism and uplift of Alpine schist in the Franz Josef – Fox Glacier area of the Southern Alps, New Zealand. *J. Metam. Geol.* **10**, 171–180.
- GRAY, D.R. & FOSTER, D.A. (2004):  $^{40}\text{Ar}/^{39}\text{Ar}$  thermochronologic constraints on deformation, metamorphism and cooling/exhumation of a Mesozoic accretionary wedge, Otago Schist, New Zealand. *Tectonophysics* **385**, 181–210.
- GUIDOTTI, C.V. (1970): The mineralogy and petrology of the transition from the lower to upper Sillimanite zone in the Oquossoc area, Maine. *J. Petrol.* **11**, 277–336.
- HALL, A.J. (1986): Pyrite–pyrrhotine redox reactions in nature. *Mineral. Mag.* **50**, 223–229.
- HALL, A.J., BOYCE, A.J. & FALICK, A.E. (1987): Iron sulphides in metasediments: isotopic support for a retrogressive pyrrhotite to pyrite reaction. *Chem. Geol.* **65**, 305–310.
- HARLOV, D.E. & HANSEN, E.C. (2005): Oxide and sulphide isograds along a Late Archean, deep-crustal profile in Tamil Nadu, south India. *J. Metam. Geol.* **23**, 241–259.
- HARLOV, D.E., NEWTON, R.C., HANSEN, E.C. & JANARDHAN, A.S. (1997): Oxide and sulphide minerals in highly oxidised, Rb-depleted, Archaean granulites of the Shevaroy Hills Massif, South India: oxidation states and the role of metamorphic fluids. *J. Metam. Geol.* **15**, 701–717.
- ITAYA, T. (1975): Pyrrhotite from Sanbagawa pelitic schists of the Shiragayama area, central Shikoku, Japan. *Mineral. J.* **8**, 25–37.
- JAMIESON, R.A. & CRAW, D. (1987): Sphalerite geobarometry in metamorphic terranes: an appraisal with implications for metamorphic pressure in Otago Schist. *J. Metam. Geol.* **5**, 87–99.
- KAWAKAMI, T., ELLIS, D.J. & CHRISTY, A.G. (2006): Sulfide evolution in high-temperature to ultrahigh-temperature metamorphic rocks from Lützow–Holm Complex, East Antarctica. *Lithos* **92**, 431–446.

- LITTLE, T.A., MORTIMER, N. & MCWILLIAMS, M.O. (1999): An episodic Cretaceous cooling model for the Otago–Marlborough schist, New Zealand, based on  $^{40}\text{Ar}/^{39}\text{Ar}$  white-mica ages. *N.Z. J. Geol. Geophys.* **42**, 305–325.
- MACKINNON, T.C. (1983): Origin of the Torlesse Terrane and coeval rocks, South Island, New Zealand. *Geol. Soc. Am., Bull.* **94**, 967–985.
- MCKEAG, S.A., CRAW, D. & NORRIS, R.J. (1989): Origin and deposition of graphitic schist-hosted metamorphogenic Au–W deposit, Macraes, East Otago, New Zealand. *Mineral. Deposita* **24**, 124–131.
- MOHR, D.W. & NEWTON, R.C. (1983): Kyanite–staurolite metamorphism in sulfidic schists of the Anakeesta Formation, Great Smoky Mountains, North Carolina. *Am. J. Sci.* **238**, 97–134.
- MORTIMER, N. (1993): Geological map of the Otago schist and adjacent rocks, scale 1:500 000. Inst. Geol. Nucl. Sci., Lower Hutt, New Zealand.
- MORTIMER, N. (2000): Metamorphic discontinuities in orogenic belts: example of the garnet – biotite – albite zone in the Otago schist, New Zealand. *Int. J. Earth. Sci.* **89**, 295–306.
- MORTIMER, N. & ROSER, B.P. (1992): Geochemical evidence for the position of the Caples–Torlesse boundary in the Otago Schist, New Zealand. *J. Geol. Soc. Lond.* **149**, 967–977.
- NORRIS, R.J., KOONS, P.O. & COOPER, A.F. (1990): The obliquely-convergent plate boundary in the South Island of New Zealand: implications for ancient collision zones. *J. Struct. Geol.* **12**, 715–725.
- PITCAIRN, I.K. (2004): *Sources of Fluids And Metals In Orogenic Gold Deposits: the Otago Schists, New Zealand*. Ph.D. thesis, Univ. of Southampton, Southampton, U.K.
- PITCAIRN, I.K., ASHLEY, M.R., TEAGLE, D.A.H., GREEN, D.R.H., CROUDACE, I.W., BREWER, T.S. & CRAW, D. (2003): Mobility of Hg, As, Sb, S and C in a metamorphic belt: insights into the source of elements enriched in orogenic gold deposits, the Otago Schists, New Zealand. In *Mineral Exploration and Sustainable Development* (G. Eliopoulos, ed.). Proc. 7<sup>th</sup> Biennial SGA meeting, Athens, Greece. Millpress, Rotterdam, The Netherlands (803–806).
- PITCAIRN, I.K., ROBERTS, S., TEAGLE, D.A.H. & CRAW, D. (2005b): Detecting hydrothermal graphite deposition during metamorphism and gold mineralization. *J. Geol. Soc. Lond.* **162**, 429–432.
- PITCAIRN, I.K., TEAGLE, D.A.H., CRAW, D., OLIVO, G.R., KERRICH, R. & BREWER, T.S. (2006a): Sources of metals and fluids in orogenic gold deposits: insights from the Otago and Alpine schists, New Zealand. *Econ. Geol.* **101**, 1525–1546.
- PITCAIRN, I.K., TEAGLE, D.A.H., KERRICH, R., CRAW, D. & BREWER, T.S. (2005a): The behaviour of nitrogen and nitrogen isotopes during metamorphism and mineralization: evidence from the Otago and Alpine schists, New Zealand. *Earth Planet. Sci. Lett.* **233**, 229–246.
- PITCAIRN, I.K., WARWICK, P.E., MILTON, J.A. & TEAGLE, D.A.H. (2006b): Method for ultra-low level analysis of gold in rocks. *Anal. Chem.* **78**, 1290–1295.
- POULSON, S.R. & OHMOTO, H. (1989): Devolatilisation equilibria in graphite–pyrite–pyrrhotite bearing pelites with application to magma–pelite interaction. *Contrib. Mineral. Petrol.* **101**, 418–425.
- RAISWELL, R. & PLANT, J. (1980): The incorporation of trace-elements into pyrite during diagenesis of black shales, Yorkshire, England. *Econ. Geol.* **75**, 684–699.
- ROSER, B.P. & COOPER, A.F. (1990): Geochemistry and terrane affiliation of the Haast Schist from the western Southern Alps, New Zealand. *N.Z. J. Geol. Geophys.* **33**, 1–10.
- RUMBLE, D., III (1973): Oxide minerals in metamorphic rocks. In *Oxide Minerals* (A. El Goresy, S.E. Haggerty, J.S. Huebner, D.H. Lindsley & D. Rumble III, eds.). *Mineral. Soc. Am., Short Course Notes* **3**, 1–24.
- SPEAR, F.S. (1993): *Metamorphic Phase Equilibria and Pressure – Temperature – Time Paths*. Mineralogical Society of America, Washington, D.C.
- SWEENEY, R.E. & KAPLAN, I.R. (1973): Pyrite framboid formation: laboratory synthesis and marine sediments. *Econ. Geol.* **68**, 618–634.
- TEAGLE, D.A.H., NORRIS, R.J. & CRAW, D. (1990): Structural controls on gold-bearing quartz mineralization in a duplex thrust system, Hyde–Macraes shear zone, Otago Schist, New Zealand. *Econ. Geol.* **85**, 1711–1719.
- THOMPSON, J.B., JR. (1972): Oxides and sulfides in regional metamorphism of pelitic schists. *Proc. 24<sup>th</sup> Int. Geol. Congress, Sect. 10*, 27–35.
- TOMKINS, A. (2010): Windows of metamorphic sulfur liberation in the crust: implications for gold deposit genesis. *Geochim. Cosmochim. Acta* **74**, 3246–3259.
- TRACY, R.J. & ROBINSON, P. (1988): Silicate – sulfide – oxide – fluid reactions in granulite grade pelitic rocks, central Massachusetts. *Am. J. Sci.* **288-A**, 45–74.
- WATSON, J.H.P., ELLWOOD, D.C., DENG, QIXI, MIKHALOVSKY, S., HAYTER, C.E. & EVANS, J. (1995): Heavy metal adsorption on bacterially produced FeS. *Mineral. Eng.* **8**, 1097–1108.
- WILKIN, R.T. & BARNES, H.L. (1997): Formation processes of framboidal pyrite. *Geochim. Cosmochim. Acta* **61**, 323–339.

Received December 3, 2009, revised manuscript accepted September 15, 2010.

